

Augmented Affine Frequency Division Multiplexing for Both Low PAPR Signaling and Diversity Gain Protection

Zhou Lu, Mohammed El-Hajjar, *Senior Member, IEEE*, and Lie-liang Yang,
Fellow, IEEE,

Abstract

Research results on Affine Frequency Division Multiplexing (AFDM) reveal that it experiences the same Peak-to-Average Power Ratio (PAPR) problem as conventional Orthogonal Frequency-Division Multiplexing (OFDM). On the other side, some references and also our studies demonstrate that AFDM involves an unneeded matrix, which is based on a parameter typically represented by c_2 , for signalling. Hence, in this paper, an augmented AFDM scheme, referred to as A²FDM, is proposed to mitigate the PAPR problem of AFDM, which is achieved by replacing the c_2 matrix in AFDM by a new unitary matrix that performs both sub-block-based Discrete Fourier Transform (DFT) and symbol mapping. Two symbol mapping schemes, namely interleaved mapping and localized mapping, are proposed for implementing A²FDM, yielding the Interleaved A²FDM and Localized A²FDM. The input-output relationships of these schemes are derived and the complexity and the effects of system parameters on the performance of A²FDM along with AFDM systems are analyzed. Furthermore, simulation results are provided to demonstrate and compare comprehensively the performance of the considered schemes in conjunction with different system settings and various operational conditions. Our studies and results demonstrate that, while A²FDM is capable of circumventing the PAPR problem faced by AFDM, it is capable of attaining the achievable diversity gain, when AFDM is operated in its undesirable conditions resulting in the loss of the diversity gain available.

Index Terms

Affine frequency division multiplexing (AFDM), orthogonal frequency-division multiplexing (OFDM), peak-to-average power ratio (PAPR), augmented AFDM (A²FDM), double-selective fading, diversity gain, equalization, single-carrier, multi-carrier.

I. INTRODUCTION

Next-generation wireless systems, including Beyond Fifth Generation (B5G) and Sixth Generation (6G) wireless networks, are expected to meet the demands of communications in

The authors are with the School of Electronics and Computer Science, University of Southampton, Southampton SO17 1BJ, United Kingdom (emails: zl15n22@soton.ac.uk, {meh, lly}@ecs.soton.ac.uk). The authors would like to acknowledge the financial support of the Engineering and Physical Sciences Research Council (EPSRC) projects under grants EP/X01228X/1, EP/X04047X/1 and EP/Y037243/1, as well as the Future Telecoms Research Hub, Platform for Driving Ultimate Connectivity (TITAN).

high-mobility scenarios for high throughput, low latency, and ultra-massive connectivity [1]. Employing such capabilities is particularly crucial for the reliable communications on high-frequency bands in the environments, such as, Vehicle-to-Everything (V2X) networks, high-speed rail, and Unmanned Aerial Vehicle (UAV) systems [2]. As a typical classic multicarrier technique, Orthogonal Frequency Division Multiplexing (OFDM) has been widely adopted in the standardized wireless systems, which demonstrates robust performance in low to mild time-varying frequency-selective fading channels [3]. However, in high-mobility scenarios, the pronounced Doppler frequency shifts associated with multiple propagation paths exacerbate the time-varying multipath fading, leading to significant signal distortion, disrupting the orthogonality between subcarriers, and ultimately, degrading the achievable system performance reflected by throughput and reliability [4]. Moreover, OFDM struggles to achieve diversity gain in linear time-varying (LTV) channels, preventing it from achieving the optimal performance, especially, in high-mobility communications scenarios [5].

Orthogonal Time Frequency Space (OTFS), proposed by Hadani in 2017, has been regarded a prominent two-dimensional (2D) modulation scheme, which demonstrates strong resilience to Doppler frequency shifts while inheriting most of the advantages of OFDM [5]. With the aid of the Zak transform, OTFS directly maps information symbols onto the 2D delay-Doppler grids, allowing superior performance in diverse communications conditions. OTFS aided by effective equalization methods is capable of addressing the fading and time-varying challenges often encountered by OFDM, enabling full diversity provided in the time and frequency domains [6]. However, OTFS has some notable drawbacks, including the increased overhead as the result of its usage of the 2D transformations for pilot signalling and multi-user multiplexing [7].

To address the limitations of OTFS and OFDM but take their respective advantages, Ali Bemani et al. introduced the Affine Frequency Division Multiplexing (AFDM) in 2021 [8, 9]. Fundamentally, AFDM belongs to a multicarrier modulation approach innovatively built upon the framework of conventional OFDM. With AFDM, data symbols are transmitted using the orthogonal chirp signals generated from the Inverse Discrete Affine Fourier transform (IDAFT) [10]. In contrast to OFDM and also Orthogonal Chirp Division Multiplexing (OCDM) [11], AFDM offers enhanced flexibility via its tunable parameters. As shown in [10, 12], when appropriately set, these parameters allow for the efficient separation of the multipath components after the Discrete Affine Fourier transform (DAFT) at the receiver. Consequently, a comprehensive and sparse representation of the channel's delay-Doppler (DD) characteristics can be obtained, supplying potentially diversity gain. More specifically, via adapting the parameters of AFDM to the DD profile of wireless channel, AFDM is capable of spreading data symbols across the whole time-frequency plane. Hence, provided that a sufficiently powerful receiver equalizer is implemented to suppress the embedded interference, full diversity gain is available, which is comparable to the performance of OTFS [13]. Furthermore, AFDM enjoys almost-perfect compatibility with the standard OFDM, and embraces OFDM and OCDM as the special signalling schemes within its framework [3]. The superb compatibility, plus its robustness and attractive performance in the highly time-

varying channels, render AFDM as one of the promising candidate signaling waveforms for applications in high-mobility scenarios in the next generation wireless communications systems.

Research on AFDM is still in its early stages, which has already shown significant promise as a new waveform for high-mobility applications [3, 14–21]. More specifically, in literature, there are several studies that analyzed the adaptability of AFDM to various communication challenges. For instance, the modulation and demodulation techniques based on discrete Fourier transform (DFT) instead of DAFT have been studied in [14]. This allows AFDM to function as a precoded OFDM waveform, ensuing compatibility with the existing OFDM systems. To address the synchronization and channel estimation challenges in AFDM systems, the authors of [15] proposed a maximum likelihood (ML) method, which leverages the redundant information contained in the chirp-periodic prefix (CPP) for more accurate synchronization. In [16], the authors introduced a pilot-assisted channel estimation method for AFDM systems, which allows to achieve the performance comparable to that by the systems with ideal channel state information (CSI). In the context of the time-varying sparse channels, the authors of [17] compared the overhead required for channel estimation when various signalling waveforms are employed. It is shown that AFDM is capable of achieving the target mean square error (MSE) performance for channel estimation with a lower number of pilots and also a lower guard interval than the state-of-the-art single-carrier modulation (SCM), OFDM, and OTFS. AFDM has also been investigated in terms of its potential for integrated sensing and communication (ISAC) applications [18, 19, 22]. Specifically, it is demonstrated in [18] that AFDM is able to decouple the delay and Doppler effects within a relatively short time, and maintain robust sensing performance even when experiencing significant Doppler shifts. The comparative studies in [19] reveal that the ISAC systems built on OTFS, OCDM and AFDM, respectively, perform similarly for ranging and velocity estimation in terms of the MSE performance. Additionally, following OFDM, AFDM has been investigated with various index modulation schemes [20, 21, 23–25], to reveal the design trade-off among spectral-efficiency, energy-efficiency and implementation complexity.

Despite its evident potentials, AFDM, like other multicarrier communication systems, experiences the problem of high Peak-to-Average Power Ratio (PAPR) [26–28]. In principle, AFDM signals have the same PAPR level as OFDM signals, which is on the order of the number of subcarriers involved in signalling [29]. This elevated PAPR can adversely affect communication efficiency and transceiver design, including limiting communication coverage due to the PAPR-resulted reduction of average transmit power, causing nonlinear distortion - which results in out-of-band emission (OOBE) and co-channel interference, and reducing the efficiency of both digital-to-analog and analog-to-digital converters (DAC/ADC). Since AFDM shares a similar signalling structure as OFDM, many PAPR mitigation techniques originally developed for OFDM can be adapted for AFDM. However, most of these PAPR mitigation methods introduce additional computational burden or/and processing steps, which yield undesirable extra delay. Through reviewing the existing studies on AFDM and our preliminary research, we recognize that the system parameter c_1 involved in IDAFT/DAFT

plays a crucial role for AFDM systems to achieve diversity gain and, hence, improve the Bit Error Rate (BER) performance. Conversely, the parameter c_2 in the IDAFT/DAFT process has a negligible impact on the performance of AFDM systems. Building on the above-mentioned observations, in this paper, we propose an enhanced AFDM structure, namely, the Augmented AFDM (A^2FDM), for solving the PAPR problem while maintaining the merits of AFDM. Our contributions are stated as follows:

- To mitigate the PAPR problem, we propose an A^2FDM signaling scheme by replacing the matrix in AFDM, which is based on the unneeded parameter c_2 , with a new unitary matrix that performs both sub-block-based DFT and symbol mapping. Accordingly, two symbol mapping schemes are proposed, which we refer to as the interleaved A^2FDM (IA^2FDM) and localized A^2FDM (LA^2FDM).
- We analyze in detail the input-output relationships of both IA^2FDM and LA^2FDM , showing the effect of the number, represented by a new system parameter μ , of DFT sub-blocks on the PAPR and the achievable diversity order.
- Considering specifically IA^2FDM , we analyze the effect of setting parameter c_1 on the performance of IA^2FDM along with AFDM, showing that the formula in references, such as [3], for setting this parameter is only necessary but not sufficient. Hence, a c_1 value following the formula in references may result in significant loss of diversity gain in AFDM systems. However, in IA^2FDM , similarly in LA^2FDM according to its principles, this problem can be avoided via the new parameter μ , making the minimum diversity order be μ , if full diversity gain is not attainable due to the use of an inappropriate parameter c_1 .
- We analyze the PAPR of both IA^2FDM and LA^2FDM , revealing that both of them have the maximum PAPR on the order of μ , instead of the total number of subcarriers in AFDM systems.
- We also analyze the complexity of A^2FDM and compare it with that of AFDM, showing that A^2FDM transmitter has only slightly added complexity from the operations of the sub-block-based DFT, while both IA^2FDM and AFDM receivers have the same complexity, when the same receiver equalizer is employed.
- Using Matlab simulations, a set of results are provided to comprehensively validate and compare the achievable performance of IA^2FDM , LA^2FDM and AFDM systems, as well as to demonstrate the impacts from the different parameters involved in these systems.

The remainder of this paper is organized as follows: Section II briefly introduces the principles of AFDM, and demonstrates the impacts of system parameters c_1 and c_2 on the performance of AFDM systems. Section III explains the principles of general A^2FDM , followed by that of the proposed IA^2FDM and LA^2FDM schemes, along with deriving the input-output relationships of the two special schemes. Section IV presents the related analysis with respect to diversity, effect of parameters, PAPR, complexity, etc. Then, in Section V, performance results are demonstrated to compare the performance of various systems. Finally, in Section VI, we conclude the research in this paper and present some future research

directions.

II. AFFINE FREQUENCY-DIVISION MULTIPLEXING (AFDM) OVER DOUBLE-SELECTIVE FADING CHANNELS

In this section, we review the principles of AFDM communicating over the time-frequency selective, i.e., double-selective, fading channels.

A. Transmitter

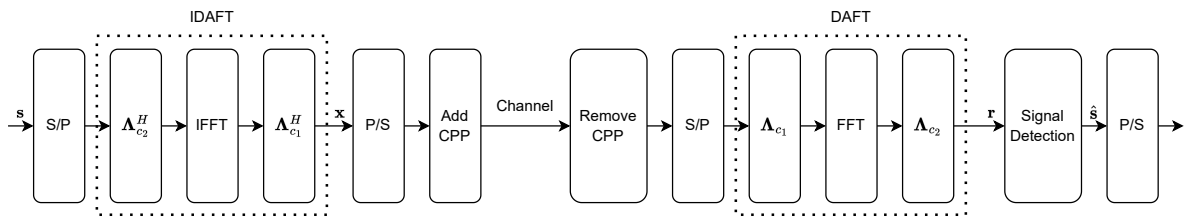


Fig. 1. Block diagram for AFDM.

In AFDM [8], Discrete Affine Frequency Transform (DAFT) is the basic building block, which is the discrete version of AFT. In general, an AFDM transceiver has the structure as shown in Fig. 1. Assume that the AFDM signalling uses N subcarriers and let $s \in \mathbb{C}^{N \times 1}$ denote the vector of information symbols generated by, such as, Quadrature Amplitude Modulation (QAM) or Phase-Shift Keying (PSK) modulation. Then, as shown in Fig. 1, after the N -point inverse DAFT (IDAFT) on s , the N number of time-domain samples can be expressed as [3]

$$x_n = \frac{1}{\sqrt{N}} \sum_{m=0}^{N-1} e^{j2\pi(c_1 n^2 + \frac{mn}{N} + c_2 m^2)} s_m, \quad n = 0, \dots, N-1. \quad (1)$$

Eq. (1) can be written in a product form as

$$x_n = e^{j2\pi c_1 n^2} \times \left[\frac{1}{\sqrt{N}} \sum_{m=0}^{N-1} e^{j\frac{2\pi mn}{N}} \left(e^{j2\pi c_2 m^2} \times s_m \right) \right], \quad n = 0, \dots, N-1. \quad (2)$$

Comparing it with the time-domain samples in OFDM [30], which is $x_n = \frac{1}{\sqrt{N}} \sum_{m=0}^{N-1} e^{j\frac{2\pi mn}{N}} s_m$, $n = 0, \dots, N-1$, we can understand that the two extra operations of AFDM on OFDM are as follows:

- The m th subcarrier symbol s_m is added an extra phase of $2\pi c_2 m^2$, i.e., s_m is preprocessed with a phase rotation of $2\pi c_2 m^2$;
- The n th time-domain sample has an extra phase of $2\pi c_1 n^2$.

Alternatively, the exponential function in (1) can be expressed as

$$e^{j2\pi(c_1 n^2 + \frac{mn}{N} + c_2 m^2)} = e^{j\frac{2\pi(c_1 n N + m + c_2 m^2/n) n \Delta t}{N \Delta t}}, \quad (3)$$

where Δt is the sampling duration, which usually satisfies $\Delta t = 1/B$ with B being the total bandwidth of AFDM system. Then, we can readily realize that the subcarrier frequency of the m th subcarrier as

$$\begin{aligned} f_m(n) &= \frac{c_1 n N + m + c_2 m^2 / n}{T_s}, \\ &= \frac{m}{T_s} + \frac{c'_1 n + c_2 m^2 / n}{T_s}, \quad n = 0, 1, \dots, N-1; \quad m = 0, 1, \dots, M-1, \end{aligned} \quad (4)$$

where $T_s = N\Delta t$ is the symbol duration and $c'_1 = c_1 N$ is a constant, representing a modified system parameter of AFDM. Eq. (4) explains that the frequency of the m th subcarrier is time-varying, increasing sample-by-sample. This time-varying subcarrier frequency enables a data symbol s_m , as seen in (1), to be sent on a wide spectrum spanning many subcarriers - typically on N subcarriers if the parameters c_1 and c_2 are appropriately selected, instead of always on the m th subcarrier with frequency m/T_s in OFDM systems. During this transmission process, a data symbol s_m can benefit from both the frequency-selectivity and time-selectivity of the wireless channel to achieve diversity gain, if a proper detection scheme is employed to mitigate the embedded interference.

When all time-domain samples are considered, Eq. (1) can be written in matrix form as

$$\mathbf{x} = \mathbf{A}^H \mathbf{s} = \Lambda_{c_2}^H \mathbf{F}^H \Lambda_{c_1}^H \mathbf{s}, \quad (5)$$

where $\mathbf{x} = [x_0, x_1, \dots, x_{N-1}]^T$, $\mathbf{A} = \Lambda_{c_2} \mathbf{F} \Lambda_{c_1}$ with \mathbf{F} being the DFT matrix having entries $\frac{1}{\sqrt{N}} e^{j2\pi mn/N}$, and $\Lambda_c = \text{diag}(e^{-j2\pi cn^2}, n = 0, 1, \dots, N-1)$ is a diagonal matrix, where $c = c_1$ or c_2 .

Similar to OFDM, AFDM also needs a prefix to mitigate the effect of delay-spread due to multipath propagation. Owing to the property of chirp waveform, it has the periodicity of

$$x_{n+uN} = e^{j2\pi c_1(u^2 N^2 + 2uNn)} x_n, \quad u = 0, 1, 2, \dots, \quad (6)$$

where u is the periodic index. Due to this special periodicity, the prefix, referred to as chirp-periodic prefix (CPP), in AFDM is given as

$$x_n = e^{-j2\pi c_1(N^2 + 2Nn)} x_{n+N}, \quad n = -L_{CPP}, \dots, -1, \quad (7)$$

where L_{CPP} is the length of CPP. Explicitly, if $c_1 = 0$, the CPP is reduced to the CP in OFDM. Furthermore, similar to the requirement by the CP in OFDM, the length of CPP L_{CPP} should be an integer not less than the channel delay spread. Moreover, as to be shown in the forthcoming discourses, the introduction of CPP allows the double-selective fading channel in AFDM to be converted to an effectively periodic form that can help to obtain diversity gain.

B. Double-Selective Fading Channel

After the parallel-to-serial (P/S) conversion, as seen in Fig. 1, the signal is transmitted over wireless channel, which may be double-selective and, hence, has the impulse response

at time n given by

$$g_n(\ell) = \sum_{i=1}^L h_i e^{-j2\pi f_i n} \delta(\ell - \ell_i), \quad (8)$$

where $L \geq 1$ is the number of propagation paths and $\delta(\cdot)$ is the Dirac delta function. In (8), h_i , f_i and ℓ_i are complex gain, Doppler shift in digital frequencies - which is the Doppler shift normalized by the sampling frequency, and the integer delay, respectively, associated with the i -th path. Specifically, if the sampling duration is $\Delta t = 1/B$, the sampling frequency is B . Hence, the actual Doppler shift is approximately $f_i B = N f_i \Delta f$, where Δf is the subcarrier spacing, satisfying $B = N \Delta f$. On the other hand, the actual delay of the i -th path is about $\tau_i = \ell_i \Delta t$.

When \mathbf{x} with its CPP is transmitted over the above described channel, the received time-domain samples can be represented as

$$y_n = \sum_{\ell=0}^{\infty} x_{n-\ell} g_n(\ell) + w_n, \quad n = 0, 1, \dots, \quad (9)$$

where $w_n \sim \mathcal{CN}(0, N_0)$ is additive Gaussian noise.

Let us define $\nu_i \triangleq N f_i = \alpha_i + \beta_i$. Hence, $\nu_i \in [-\nu_{\max}, \nu_{\max}]$ is the Doppler shift normalized by the subcarrier spacing Δf , and ν_{\max} is the maximum normalized Doppler shift. Accordingly, $\alpha_i \in [-\alpha_{\max}, \alpha_{\max}]$ is the integer part of ν_i , and β_i is the fractional part of ν_i satisfying $-\frac{1}{2} \leq \beta_i \leq \frac{1}{2}$. Assume that the maximum delay of the channel satisfies $\ell_{\max} \triangleq \max(\ell_i) < N$, and the CPP length L_{CPP} is larger than $\ell_{\max} - 1$. Then, the matrix form of (9) can be written as [3]

$$\mathbf{y} = \mathbf{H}\mathbf{x} + \mathbf{w}, \quad (10)$$

where $\mathbf{w} \sim \mathcal{CN}(\mathbf{0}, N_0 \mathbf{I})$ is the additive white Gaussian noise vector, \mathbf{I} is identity matrix, while the channel matrix \mathbf{H} is given by [3]

$$\mathbf{H} = \sum_{i=1}^L h_i \Gamma_{CPP_i} \Delta_{f_i} \Pi^{\ell_i}. \quad (11)$$

Following [3], the terms in (11) are defined as follows. Γ_{CPP_i} is an $N \times N$ diagonal matrix given as

$$\Gamma_{CPP_i} = \text{diag} \left(\begin{cases} e^{-j2\pi c_1 (N^2 - 2N(\ell_i - n))}, & n < \ell_i, \\ 1, & n \geq \ell_i, \end{cases}, \quad n = 0, 1, \dots, N-1 \right), \quad (12)$$

which, for $n < \ell_i$, has the contribution of the phase shifts induced by the CPP. When $n \geq \ell_i$, CPP has no effect on the signal, and hence the diagonal elements of Γ_{CPP_i} are equal to 1. $\Delta_{f_i} \triangleq \text{diag}(e^{-j2\pi f_i n}, n = 0, 1, \dots, N-1)$ accounts for the effect of the Doppler shifts, while Π^{ℓ_i} explains the effect of delay ℓ_i of the ℓ_i -th path, where Π is a forward cyclic-shift matrix expressed as [8]

$$\Pi = \begin{bmatrix} 0 & \dots & 0 & 1 \\ 1 & \dots & 0 & 0 \\ \vdots & \ddots & \ddots & \vdots \\ 0 & \dots & 1 & 0 \end{bmatrix}_{N \times N}. \quad (13)$$

C. Demodulation

As shown in Fig. 1, for the receiver to demodulate the information symbols, the DAFT is firstly carried out on the received signal in (10), which can be expressed as

$$\begin{aligned}
\mathbf{r} &= \mathbf{A}\mathbf{y} = \mathbf{A} \left(\sum_{i=1}^L h_i \mathbf{\Gamma}_{CPP_i} \mathbf{\Delta}_{f_i} \mathbf{\Pi}^{\ell_i} \right) \mathbf{A}^H \mathbf{s} + \mathbf{w}' \\
&= \sum_{i=1}^L h_i \mathbf{H}_{eff}^{(i)} \mathbf{s} + \mathbf{w}' \\
&= \mathbf{H}_{eff} \mathbf{s} + \mathbf{w}',
\end{aligned} \tag{14}$$

where, by definition, $\mathbf{H}_{eff}^{(i)} = \mathbf{A} \mathbf{\Gamma}_{CPP_i} \mathbf{\Delta}_{f_i} \mathbf{\Pi}^{\ell_i} \mathbf{A}^H$, $\mathbf{H}_{eff} = \mathbf{A} \mathbf{H} \mathbf{A}^H$ accounts for the effective end-to-end channel, where $\mathbf{H} = \sum_{i=1}^L h_i \mathbf{\Gamma}_{CPP_i} \mathbf{\Delta}_{f_i} \mathbf{\Pi}^{\ell_i}$, and $\mathbf{w}' = \mathbf{A}\mathbf{w}$.

In (14), \mathbf{H}_{eff} is not a diagonal matrix, and the columns of \mathbf{H}_{eff} are also not orthogonal. Hence, the symbols in \mathbf{s} interfere with each other. Consequently, more complex equalization than that in the conventional OFDM systems is required. In literature, various detection schemes have been proposed and studied [31–33], including MRC-based detection and pilot aided detection. Specifically, when a linear minimum mean-square error (MMSE) equalizer is employed, the decision variables can be formed as

$$\mathbf{y} = \mathbf{W}^H \mathbf{r}, \tag{15}$$

where the weight matrix \mathbf{W} can be derived from (14) and is expressed as

$$\mathbf{W} = \left(\mathbf{H}_{eff} \mathbf{H}_{eff}^H + \frac{1}{\gamma} \mathbf{I} \right)^{-1} \mathbf{H}_{eff}, \tag{16}$$

where γ is the signal-to-noise ratio (SNR) per symbol.

TABLE I
PARAMETERS FOR SIMULATIONS OF AFDM AND A²FDM.

Parameter	Value
Light speed	$c = 3 \times 10^8$ m/s
Carrier frequency	$f_c = 3.5$ GHz
Subcarrier spacing	$\Delta f = 30$ kHz
Velocity of user	$v = 100$ kilometers/hour (km/h)
Number of subcarriers	$N = 256$
Number of channel paths	$L = 10$
Modulation	4QAM

The researches [3, 8, 9] show that the system parameter c_1 imposes a big impact on the achievable performance of AFDM systems. Specifically, to obtain the full diversity gain, c_1 should be chosen a value of

$$c_1 > \left(c_{1f} = \frac{2\nu_{\max}}{2N \times \min(|\ell_j - \ell_i|)} \right), \tag{17}$$

where c_{1f} is the minimum value of c_1 required for the AFDM system to achieve full diversity. This is also illustrated in Fig. 2, which compares the BER performance of the same AFDM system but with different values for the parameter c_1 . The simulation parameters are detailed in Table I, unless otherwise specified. In our simulations, all channel paths are assumed to experience Rayleigh fading with a common power $1/L$.

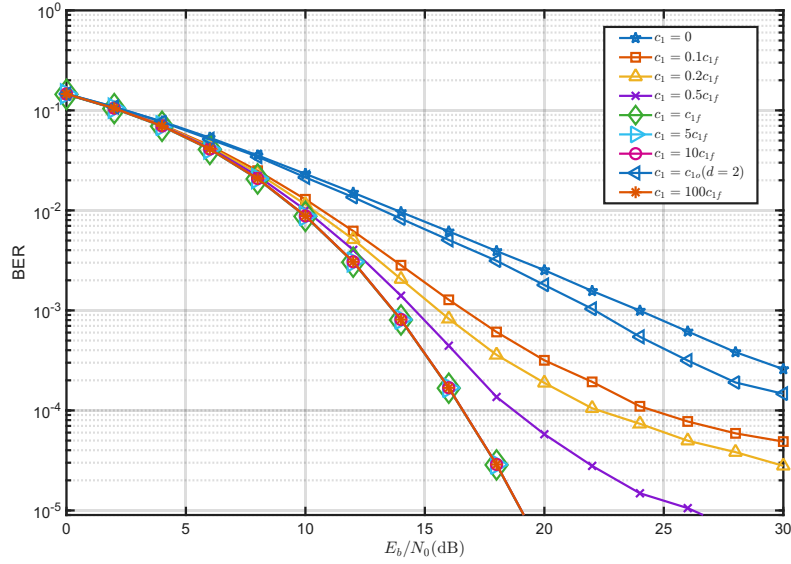


Fig. 2. BER performance of AFDM system with MMSE equalization, with the settings of $f_c = 3.5\text{GHz}$, $\Delta f = 30\text{ kHz}$, $v = 100\text{ km/h}$, $N = 256$, $L = 10$, 4QAM, and $c_2 = 0$.

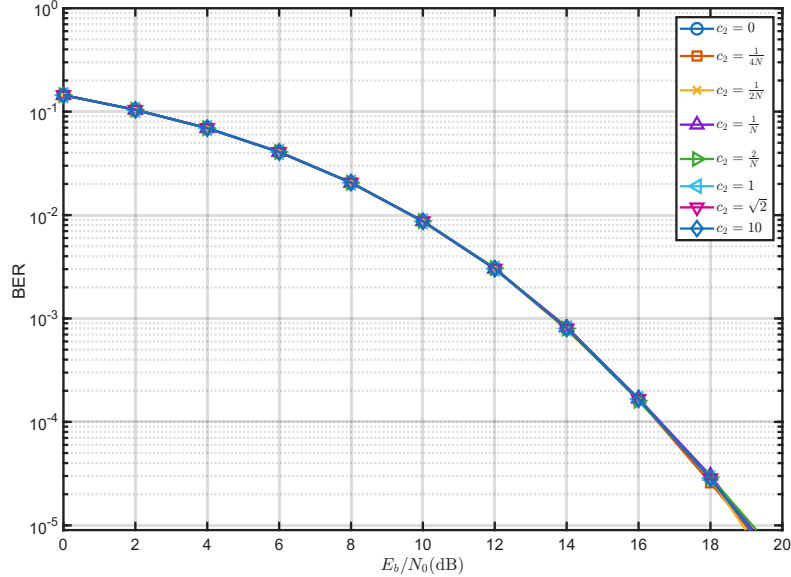


Fig. 3. BER performance of AFDM systems with MMSE equalization and $c_1 = c_{1f}$.

The results in Fig. 2 show that the BER performance of AFDM is strongly relied on the value of c_1 . The BER performance improves with the increase of c_1 until $c_1 = c_{1f}$. Then,

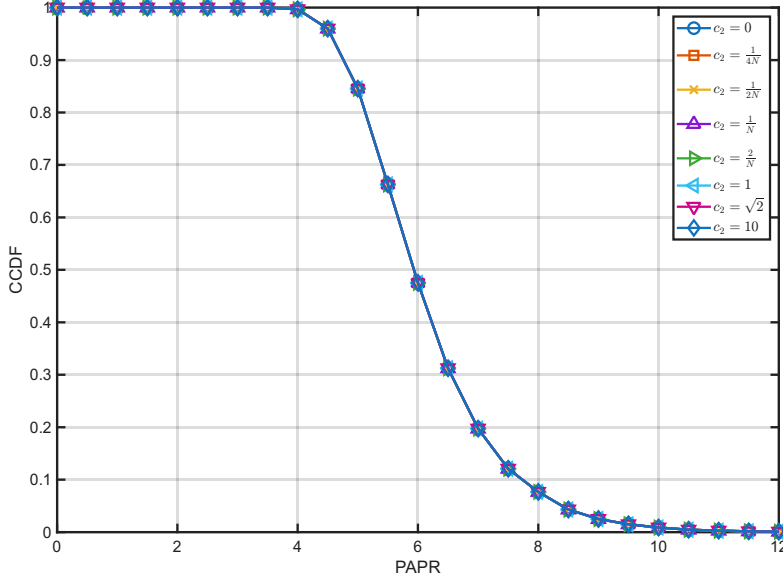


Fig. 4. PAPR of AFDM transmit signals with $c_1 = c_{1f}$.

further increasing c_1 has little effect on the BER performance of the AFDM system, unless a big but inappropriate c_1 value, as shown by the curve corresponding to “ $c_1 = c_{1o}(d = 2)$ ”, which will be addressed in Section IV-A.

In contrast to c_1 having a big impact on the BER performance of AFDM systems, the parameter c_2 yields little effect, which has already been realized in some references. For example, in [3], it is noted that optimum diversity order can be achieved, provided that c_2 is chosen to be an irrational number or a small rational number. Moreover, the parameter c_2 is simply ignored in the transmitter design in [10]. To illustrate the insignificance of parameter c_2 , we present Fig. 3 and Fig. 4 to show its effect on the BER and PAPR performance, respectively, of AFDM systems. The main parameters are the same as that shown in Table I. As shown in Fig. 3, for a given value of $c_1 = c_{1f}$, different values of c_2 generate nearly the same performance. It is worth noting that the BER performance is nearly the same, even when c_2 is not small but as big as 10. The PAPR results in Fig. 4 show that c_2 has no effect at all, no matter what value it is set. Therefore, in general, the diagonal matrix contributed by parameter c_2 can be removed from AFDM systems. Note that, as the application of c_1 only shifts signals in the frequency-domain, as to be shown by the analysis in Section III-A1, it has no effect on PAPR.

However, AFDM experiences the same PAPR problem as OFDM, which should be mitigated, especially, when uplink communications are implemented. Accordingly, in this paper, we enhance the design of AFDM to not only attain full diversity gain, but also significantly reduce the PAPR of transmit signals.

III. AUGMENTED AFDM (A²FDM)

We propose the A²FDM to serve two purposes. The first is to reduce the PAPR conflicted by AFDM, as above-mentioned. In AFDM, especially, when the number of channel paths is relatively small, the selection of parameter c_1 is dependent on the knowledge about the delays and Doppler shifts, as seen in Eqs. (45) - (48) in [3], which may not be always available in practice. Furthermore, in practical mobile communications, delays and Doppler shifts as well as their distributions are time-varying, meaning that a fixed value of c_1 may never be optimal. Therefore, it is important to set c_1 a value that is robust in different communication environments. Hence, the second purpose is to enable A²FDM systems to achieve the near-optimum performance in terms of diversity gain (orders) for any randomly selected c_1 value.

The fundamental principle of A²FDM is to replace the c_2 -related diagonal matrix in AFDM by a block-diagonal matrix with component DFT matrices, as detailed in the following subsection.

A. Transmitter of A²FDM

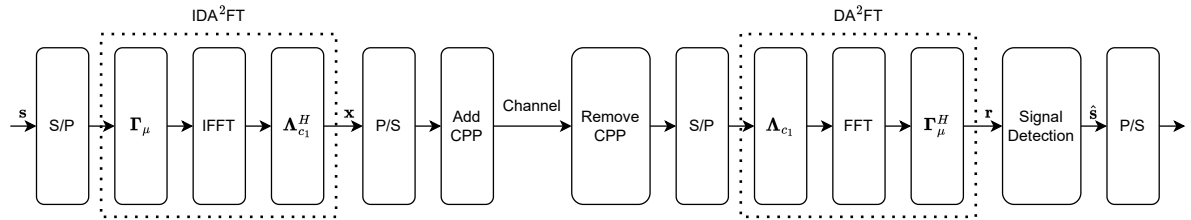


Fig. 5. Block diagram of A²FDM.

Along with OFDM, although various PAPR reduction methods have been proposed [26, 34–37], they usually introduce significant extra processes, which are not desirable. Hence, to reduce the PAPR of AFDM and further enhance its flexibility in implementation, but without significant increase of implementation cost, we introduce an augmented AFDM, referred to as A²FDM, scheme, by exploiting the principles of single-carrier frequency-division multiple-access (SC-FDMA) [30].

Specifically, as shown in Fig. 5, instead of the DAFT in AFDM, our A²FDM scheme relies on a so-called discrete augmented affine Fourier transform (DA²FT) with the operator expressed as

$$\mathbf{A} = \mathbf{\Gamma}_\mu^H \mathbf{F} \mathbf{\Lambda}_{c_1}, \quad (18)$$

where $\mathbf{\Gamma}_\mu$ is chosen to make \mathbf{A} a unitary matrix, i.e., satisfying $\mathbf{A}\mathbf{A}^H = \mathbf{A}^H\mathbf{A} = \mathbf{I}$. Since in this paper, one of our design objectives is to solve the PAPR problem of AFDM, following the principles of SC-FDMA [30], we design $\mathbf{\Gamma}_\mu$ as

$$\mathbf{\Gamma}_\mu = \mathbf{P} \mathbf{\Upsilon}_\mu. \quad (19)$$

Again, assume that the total number of subcarriers is N . Then, in (19), Υ_μ is a $N \times N$ block-diagonal matrix consisting of μ number of component FFT matrices of $N_\mu \times N_\mu$ dimensions, i.e.,

$$\begin{aligned}\Upsilon_\mu &= \text{diag}\left(\underbrace{\mathbf{F}_{N_\mu}, \mathbf{F}_{N_\mu}, \dots, \mathbf{F}_{N_\mu}}_\mu\right) \\ &= \mathbf{I}_\mu \otimes \mathbf{F}_{N_\mu},\end{aligned}\quad (20)$$

where \otimes is Kronecker product, \mathbf{F}_{N_μ} is a $N_\mu \times N_\mu$ normalized FFT matrix, $N_\mu = N/\mu$ is an integer, preferably equalling to 2^i for convenience of FFT implementation. In (19), \mathbf{P} is a $N \times N$ permutation matrix implementing the mapping of signals to different subcarriers, so that signal power is redistributed to attain a lower PAPR after IFFT. Following the interleaved FDMA and localized FDMA in SC-FDMA [30], in this paper, both the interleaved permutation and localized permutation are considered, resulting in the Interleaved A²FDM (IA²FDM) and Localized A²FDM (LA²FDM) schemes. Since \mathbf{P} is a permutation matrix, it satisfies $\mathbf{P}^T \mathbf{P} = \mathbf{P} \mathbf{P}^T = \mathbf{I}$. Therefore, we can readily show that DA²FT matrix defined in (18) is a unitary matrix.

Note that in (20), we assumed that all the component FFT matrices in Υ_μ have the same dimensions, for the sake of simplicity of the forthcoming analysis. However, it is worth noting that its extension to including the component FFT matrices of various sizes is straightforward. This is practically the case, when a base-station (BS) sends information to its downlink users at different rates, or when different uplink users communicate with a BS at different rates. In both cases, different users may be assigned different amount of resources, such as different numbers of subcarriers.

Corresponding to the structure of Υ_μ , the N data symbols, such as QAM/PSK symbols, to be transmitted are divided into μ groups of each having N_μ symbols, expressed as $\mathbf{s} = [\mathbf{s}_0^T, \mathbf{s}_1^T, \dots, \mathbf{s}_{\mu-1}^T]^T$. Let us express $\mathbf{z} = \Upsilon_\mu \mathbf{s}$. Then, according to \mathbf{s} , \mathbf{z} can be divided into $\mathbf{z} = [\mathbf{z}_0^T, \mathbf{z}_1^T, \dots, \mathbf{z}_{\mu-1}^T]^T$, where \mathbf{z}_k is a N_μ -length vector given by

$$\mathbf{z}_k = \mathbf{F}_{N_\mu} \mathbf{s}_k, \quad k = 0, 1, \dots, \mu - 1. \quad (21)$$

More specifically, the p -th element of \mathbf{z}_k is given by

$$z_{kp} = \frac{1}{\sqrt{N_\mu}} \sum_{l=0}^{N_\mu-1} s_{kl} e^{-j2\pi \frac{pl}{N_\mu}}, \quad p = 0, 1, \dots, N_\mu - 1, \quad (22)$$

where symbol s_{kl} is the l -th element in \mathbf{s}_k , which is the symbol of $\mathbf{s}_{kN_\mu+l}$ in \mathbf{s} for $k = 0, 1, \dots, \mu - 1$ and $l = 0, 1, \dots, N_\mu - 1$. Hence, the entries in $\mathbf{z} = \Upsilon_\mu \mathbf{s}$ can be expressed as

$$\begin{aligned}z_{kN_\mu+p} &= \frac{1}{\sqrt{N_\mu}} \sum_{l=0}^{N_\mu-1} s_{kN_\mu+l} e^{-j2\pi \frac{(kN_\mu+p)(kN_\mu+l)}{N_\mu}} \\ &= \frac{1}{\sqrt{N_\mu}} \sum_{l=0}^{N_\mu-1} s_{kN_\mu+l} e^{-j2\pi \frac{pl}{N_\mu}}\end{aligned}\quad (23)$$

for all $p = 0, 1, \dots, N_\mu - 1$ and $k = 0, 1, \dots, \mu - 1$.

Following the FFT, symbol permutation is carried out via multiplying matrix \mathbf{P} on \mathbf{z} . Hence, different permutation strategies may be implemented via designing \mathbf{P} . Following the IFDMA and LFDMA in SC-FDMA [30], in this paper, we propose the concepts of the IA²FDM and LA²FDM, which are detailed in the following sections.

1) *IA²FDM*: With IA²FDM, the N_μ symbols in \mathbf{z}_k are evenly mapped via permutation onto N_μ subcarriers of the whole $N = \mu N_\mu$ subcarriers. After the subcarrier mapping, the transmitter forms an extended N -length symbol vector. Specifically, corresponding to \mathbf{z}_k , the mapping operation obeys

$$\begin{aligned} \mathbf{g} &= [g_0, g_1, \dots, g_{N-1}]^T \\ &= \mathbf{P}_k \mathbf{z}_k, \end{aligned} \quad (24)$$

where \mathbf{P}_k is responsible for the mapping of the entries in \mathbf{z}_k , which constitutes the N_μ columns of \mathbf{P} that match to the positions of \mathbf{z}_k in \mathbf{z} . Let us set $\mathbf{z}_k = [z_{k0}, z_{k1}, \dots, z_{k(N_\mu-1)}]^T$ for $k = 0, 1, \dots, \mu - 1$. Then, when IA²FDM is implemented, \mathbf{P}_k is designed to set the value of g_m according to

$$g_m = \begin{cases} z_{kp}, & m = p\mu + k, \\ 0, & \text{otherwise.} \end{cases} \quad (25)$$

Hence, to implement the interleaved permutation, the columns of the permutation matrix \mathbf{P} can be constructed as

$$\mathbf{P}(:, kN_\mu + p) = \mathbf{I}_N(:, p\mu + k), \quad (26)$$

for $p = 0, 1, \dots, N_\mu - 1$ and $k = 0, 1, \dots, \mu - 1$, where \mathbf{I}_N is a $N \times N$ identity matrix. Let $\mathbf{g} = \mathbf{P}\mathbf{z} = \Gamma_\mu \mathbf{s}$. Then, according to (26), the element at $kN_\mu + p$ in \mathbf{z} is mapped to the position $p\mu + k$ in \mathbf{g} , i.e., $g_{p\mu+k} = z_{kN_\mu+p}$ for $p = 0, 1, \dots, N_\mu - 1$ and $k = 0, 1, \dots, \mu - 1$.

An example of \mathbf{P} implementing interleaved permutation with $N = 16$ and $\mu = 2$ is shown in Fig. 6, where a shaded box represents an element 1 and, otherwise, the element value is 0. As shown in Fig. 6, the symbols from 2 groups are alternatively allocated to the 16 subcarriers.

After the permutation operation, the remaining transmitter operations in IA²FDM are the same as that in AFDM, including the IFFT, the phase shifting operation invoking parameter c_1 , adding CPP, etc. It can be shown that the n th sample in the transmitted signal \mathbf{x} can be expressed as

$$\begin{aligned} x_n &= \frac{1}{\sqrt{N}} \sum_{p\mu+k=0}^{N-1} g_{p\mu+k} e^{j2\pi(c_1 n^2 + \frac{(p\mu+k)n}{N})} \\ &= \frac{1}{\sqrt{N}} e^{j2\pi c_1 n^2} \sum_{p\mu+k=0}^{N-1} z_{kN_\mu+p} e^{j2\pi \frac{(p\mu+k)n}{N}} \\ &= \frac{1}{\sqrt{N}} e^{j2\pi c_1 n^2} \sum_{k=0}^{\mu-1} e^{j2\pi \frac{kn}{N}} \sum_{p=0}^{N_\mu-1} z_{kN_\mu+p} e^{j2\pi \frac{pn}{N_\mu}}, \quad n = 0, 1, \dots, N-1. \end{aligned} \quad (27)$$

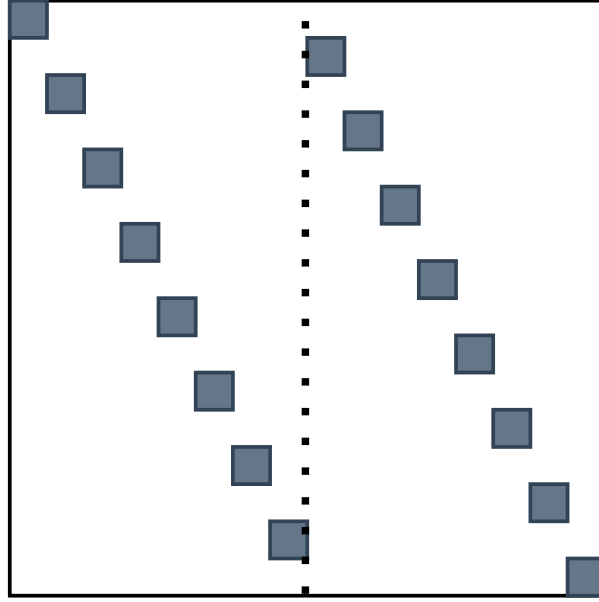


Fig. 6. Structure of matrix \mathbf{P} for IA²FDM with $\mu = 2$.

Denote $n = aN_\mu + b$ with $a = 0, 1, \dots, \mu - 1$ and $b = 0, 1, \dots, N_\mu - 1$. Then, (27) can be written as

$$\begin{aligned}
 x_{(aN_\mu + b)} &= \frac{1}{\sqrt{N}} e^{j2\pi c_1(aN_\mu + b)^2} \sum_{k=0}^{\mu-1} e^{j2\pi \frac{k(aN_\mu + b)}{N}} \sum_{p=0}^{N_\mu-1} z_{kN_\mu + p} e^{j2\pi \frac{p(aN_\mu + b)}{N_\mu}} \\
 &= \frac{1}{\sqrt{\mu}} e^{j2\pi c_1(aN_\mu + b)^2} \sum_{k=0}^{\mu-1} e^{j2\pi \frac{k(aN_\mu + b)}{N}} \frac{1}{\sqrt{N_\mu}} \sum_{p=0}^{N_\mu-1} z_{kN_\mu + p} e^{j2\pi \frac{paN_\mu + pb}{N_\mu}} \\
 &= \frac{1}{\sqrt{\mu}} e^{j2\pi c_1(aN_\mu + b)^2} \sum_{k=0}^{\mu-1} e^{j2\pi \frac{k(aN_\mu + b)}{N}} s_{kN_\mu + b}.
 \end{aligned} \tag{28}$$

Hence, when substituting $n = aN_\mu + b$ back into (28) and denoting $m = kN_\mu + b$, the time-domain samples can be expressed as

$$x_n = \frac{1}{\sqrt{\mu}} e^{j2\pi c_1 n^2} \sum_{k=0}^{\mu-1} s_m e^{j2\pi \frac{kn}{N}}, \quad n = 0, 1, \dots, N - 1. \tag{29}$$

Accordingly, the continuous-time signal can be expressed as

$$x(t) = \sqrt{\frac{P}{\mu}} \sum_{k=0}^{\mu-1} s_m e^{j2\pi \frac{(c_1 N n + k)t}{T_s}}, \tag{30}$$

where P is transmit power and T_s is symbol duration. (30) shows that, at any time, there are only μ active subcarriers, which includes the frequencies given by $(c_1 N n + k)/T_s$, determined by both k and $c_1 N n$. Therefore, the PAPR of A²FDM can be significantly lower than that of AFDM.

2) **LA²FDM**: When the LA²FDM is implemented, the N_μ symbols in \mathbf{z}_k obtained from the N_μ -point FFT processing are assigned to N_μ successive subcarriers, which can be formulated as

$$g_m = \begin{cases} z_{kp}, & m = kN_\mu + p, \quad p = 0, 1, \dots, N_\mu - 1 \\ 0, & \text{otherwise,} \end{cases} \quad (31)$$

Hence, matrix \mathbf{P} is simply an identity matrix \mathbf{I}_N , and \mathbf{P}_k is just constituted by the N_μ columns corresponding to \mathbf{z}_k , yielding

$$g_{kN_\mu+p} = z_{kN_\mu+p}, \quad p = 0, 1, \dots, N_\mu - 1; \quad k = 0, 1, \dots, \mu - 1. \quad (32)$$

Therefore, in LA²FDM, the samples in \mathbf{x} can be expressed as

$$\begin{aligned} x_n &= \frac{1}{\sqrt{N}} \sum_{kN_\mu+p=0}^{N-1} g_{kN_\mu+p} e^{j2\pi(c_1 n^2 + \frac{(kN_\mu+p)n}{N})} \\ &= \frac{1}{\sqrt{N}} e^{j2\pi c_1 n^2} \sum_{kN_\mu+p=0}^{N-1} z_{kN_\mu+p} e^{j2\pi \frac{(kN_\mu+p)n}{N}} \\ &= \frac{1}{\sqrt{N}} e^{j2\pi c_1 n^2} \sum_{k=0}^{\mu-1} e^{j2\pi \frac{kn}{\mu}} \sum_{p=0}^{N_\mu-1} z_{kN_\mu+p} e^{j2\pi \frac{pn}{N}}. \end{aligned} \quad (33)$$

Let us define $n = b\mu + a$ for $b = 0, 1, \dots, N_\mu - 1$ and $a = 0, 1, \dots, \mu - 1$. Then, we have

$$\begin{aligned} x_{(b\mu+a)} &= \frac{1}{\sqrt{N}} e^{j2\pi c_1 (b\mu+a)^2} \sum_{k=0}^{\mu-1} e^{j2\pi \frac{k(b\mu+a)}{\mu}} \sum_{p=0}^{N_\mu-1} z_{kN_\mu+p} e^{j2\pi \frac{p(b\mu+a)}{N}} \\ &= \frac{1}{\sqrt{\mu}} e^{j2\pi c_1 (b\mu+a)^2} \sum_{k=0}^{\mu-1} e^{j2\pi \frac{ka}{\mu}} \frac{1}{\sqrt{N_\mu}} \sum_{p=0}^{N_\mu-1} z_{kN_\mu+p} e^{j2\pi \frac{p(b\mu+a)}{N}} \\ &= \frac{1}{\sqrt{\mu}} e^{j2\pi c_1 (b\mu+a)^2} \sum_{k=0}^{\mu-1} e^{j2\pi \frac{ka}{\mu}} x'_{(b\mu+a)}, \end{aligned} \quad (34)$$

where we defined $x'_{(b\mu+a)} = \frac{1}{\sqrt{N_\mu}} \sum_{p=0}^{N_\mu-1} z_{kN_\mu+p} e^{j2\pi \frac{p(b\mu+a)}{N}}$, which is analyzed in Appendix A, showing that

$$x'_n = \begin{cases} s_{kN_\mu+b}, & n = b\mu \quad (a = 0), \\ \frac{1}{N_\mu} \sum_{l=0}^{N_\mu-1} s_{kN_\mu+l} \left(\frac{1 - e^{j \frac{2\pi n}{\mu}}}{1 - e^{j \frac{2\pi n}{N}} e^{-j \frac{2\pi l}{N_\mu}}} \right), & \text{otherwise} \quad (a \neq 0), \end{cases} \quad (35)$$

where $b = 0, 1, \dots, N_\mu - 1$.

Upon substituting (35) into (34), the time-domain samples transmitted in LA²FDM are given by

$$x_n = \begin{cases} \frac{1}{\sqrt{\mu}} e^{j2\pi c_1 n^2} \sum_{k=0}^{\mu-1} e^{j2\pi \frac{k[n/\mu]}{\mu}} s_m, & n = b\mu, \\ \frac{1}{N_\mu \sqrt{\mu}} e^{j2\pi c_1 n^2} \sum_{k=0}^{\mu-1} e^{j2\pi \frac{k[n/\mu]}{\mu}} \sum_{l=0}^{N_\mu-1} s_m \left(\frac{1 - e^{j \frac{2\pi n}{\mu}}}{1 - e^{j \frac{2\pi n}{N}} e^{-j \frac{2\pi l}{N_\mu}}} \right), & n \neq b\mu, \end{cases} \quad (36)$$

where $[n/\mu]$ denotes the μ -modulo operation on n , and $m = kN_\mu + b = 0, 1, \dots, N-1$, when b and k scan the ranges of $b = 0, 1, \dots, N_\mu$ and $k = 0, 1, \dots, \mu-1$.

Following the IA²FDM in Section III-A1, it can be analyzed that at the times $t = b\mu\Delta t$, there are only μ subcarriers activated at frequencies $(c_1 n N + k N_\mu)/T_s$ for $k = 0, 1, \dots, \mu$. At the other times of $t \neq b\mu\Delta t$, there are more than μ active subcarriers. Specifically, for a given k , the group of N_μ symbols are transmitted on three subcarriers located at $(c_1 n N + k N_\mu)/T_s$, N_μ/T_s and μ/T_s . Therefore, the total number of subcarriers activated is $\mu+2$, owing to the fact that N_μ/T_s and μ/T_s are common to all k . Hence, it can be expected that the PAPR of LA²FDM can also be significantly lower than that of AFDM.

Finally, for both the IA²FDM and LA²FDM, the signal \mathbf{x} is formed by operating the corresponding inverse DA²FT (IDA²FT) on \mathbf{s} , yielding

$$\mathbf{x} = \mathbf{A}^H \mathbf{s} = \mathbf{\Lambda}_{c_1}^H \mathbf{F}^H \mathbf{\Gamma}_\mu \mathbf{s} = \mathbf{\Lambda}_{c_1}^H \mathbf{F}^H \mathbf{P} \mathbf{\Upsilon}_\mu \mathbf{s} \quad (37)$$

B. Input-Output Relationship

Assume the double-selective fading channels having the CIR expressed as (8). Then, the input-output relationship in A²FDM systems can also be represented by (14) after the operation of DA²FT at receiver, where \mathbf{H}_{eff} in (14) can be expressed as $\mathbf{H}_{eff} = \sum_{i=1}^L h_i \mathbf{H}_i$ and

$$\mathbf{H}_i \triangleq \mathbf{A} \mathbf{\Gamma}_{CPP_i} \mathbf{\Delta}_{f_i} \mathbf{\Pi}^{\ell_i} \mathbf{A}^H. \quad (38)$$

Below we analyze the effective channel \mathbf{H}_{eff} with the emphasis on the effect from the matrix $\mathbf{\Gamma}_\mu$. We address here the IA²FDM, which can be readily generalized to the LA²FDM.

After removing the CPP, it can be known that $\mathbf{\Gamma}_{CPP_i}$ becomes an identity matrix. In (38), $\mathbf{\Pi}^{\ell_i}$ accounts for the delay of the i -th path, which has the element values given by $\delta(o - (n - \ell_i))$, where an element of $\mathbf{\Pi}^{\ell_i}$ is 1 only if $o = n - \ell_i$ is satisfied, and otherwise, it is 0. Note that, in $\delta(o - (n - \ell_i))$, o and n denote respectively the column index and row index of $\mathbf{\Pi}^{\ell_i}$. Hence, with the above-mentioned limitations, the (p, q) -th element in \mathbf{H}_i can be analyzed as

$$H_i[p, q] = \mathbf{A}[p, n] \mathbf{\Delta}_{f_i}[n, n] \mathbf{\Pi}^{\ell_i}[n, o] \mathbf{A}^H[o, q] \quad (39a)$$

$$= \frac{1}{\sqrt{\mu}} \sum_{n=0}^{\mu-1} e^{-j2\pi(c_1 n^2 + \frac{pn}{N})} e^{-j2\pi f_i n} \delta(o - (n - \ell_i)) \frac{1}{\sqrt{\mu}} \sum_{o=0}^{\mu-1} e^{j2\pi(c_1 o^2 + \frac{qo}{N})} \quad (39b)$$

$$= \frac{1}{\mu} \sum_{n=0}^{\mu-1} e^{-j2\pi(c_1 n^2 + \frac{pn}{N} + f_i n)} e^{j2\pi(c_1 n^2 - 2c_1 \ell_i n + c_1 \ell_i^2 + \frac{qn - q\ell_i}{N})} \quad (39c)$$

$$= \frac{1}{\mu} \sum_{n=0}^{\mu-1} e^{-j2\pi(\frac{(p-q)n}{N} + f_i n + 2c_1 \ell_i n - c_1 \ell_i^2 + \frac{q\ell_i}{N})} \quad (39d)$$

$$= \frac{1}{\mu} e^{j\frac{2\pi}{N}(Nc_1 \ell_i^2 - q\ell_i)} \sum_{n=0}^{\mu-1} e^{-j\frac{2\pi n}{N}(p-q+\nu_i+2Nc_1 \ell_i)} \quad (39e)$$

$$= \frac{1}{\mu} e^{j\frac{2\pi}{N}(Nc_1 \ell_i^2 - q\ell_i)} \mathcal{F}_i(p, q), \quad (39f)$$

where from (39d) to (39e) $\nu_i = Nf_i$ was applied followed by some arrangements afterwards. By definition, $\mathcal{F}_i(p, q)$ in (39f) is

$$\begin{aligned}\mathcal{F}_i(p, q) &= \sum_{n=0}^{\mu-1} e^{-j\frac{2\pi n}{N}(p-q+\nu_i+2Nc_1\ell_i)} \\ &= \frac{1 - e^{-j\frac{2\pi\mu}{N}(p-q+\nu_i+2Nc_1\ell_i)}}{1 - e^{-j\frac{2\pi}{N}(p-q+\nu_i+2Nc_1\ell_i)}} \\ &= \frac{1 - e^{-j\frac{2\pi}{N\mu}(p-q+\nu_i+2Nc_1\ell_i)}}{1 - e^{-j\frac{2\pi}{N}(p-q+\nu_i+2Nc_1\ell_i)}},\end{aligned}\tag{40}$$

which is dependent on the Doppler shift $\nu_i = \alpha_i + \beta_i$. As seen, ν_i includes an integer part α_i and a fractional part β_i , both imposing effect on $\mathcal{F}_i(p, q)$, as analyzed below.

1) *Integer Doppler Shifts*: In this case, $\beta_i = 0$ and $\nu_i = \alpha_i$. Define $\vartheta = e^{-j\frac{2\pi}{N}(p-q+\nu_i+2Nc_1\ell_i)}$.

Then, we can obtain

$$\mathcal{F}_i(p, q) = \begin{cases} \mu, & \vartheta = 1, \\ 0, & \vartheta \neq 1. \end{cases}\tag{41}$$

To get $\vartheta = 1$, $p - q + \alpha_i + 2Nc_1\ell_i$ should be an integer that is a multiple of N , leading to $p = [(\alpha_i + 2Nc_1\ell_i - q)/N]$. Accordingly, (39) becomes

$$H_i[p, q] = \begin{cases} e^{j\frac{2\pi}{N}(Nc_1\ell_i^2 - q\ell_i)}, & p = [(\eta_i - q)/N] \\ 0, & \text{otherwise,} \end{cases}\tag{42}$$

where $\eta_i = [(\alpha_i + 2Nc_1\ell_i)/N]$. Therefore, in row p of \mathbf{H}_i , there is only one non-zero element, whose column number q satisfies $p = [(\eta_i - q)/N]$. Consequently, $r(p)$ of the received signal \mathbf{r} seen in the input-output relationship can be represented as

$$r[p] = \sum_{i=1}^L h_i e^{j\frac{2\pi}{N}(Nc_1\ell_i^2 - q\ell_i)} s[q] + \tilde{w}[p], \quad p = 0, 1, \dots, N-1,\tag{43}$$

where q satisfies $p = [(\eta_i - q)/N]$.

2) *Fractional Doppler Shifts*: In the case of fractional Doppler shifts, $-1/2 < \beta_i \leq 1/2$ in $\nu_i = \alpha_i + \beta_i$. Hence, ϑ cannot be an integer value. Accordingly, (40) can be simplified to an expression of

$$\mathcal{F}_i(p, q) = \frac{1 - e^{-j2\pi\mu\theta}}{1 - e^{-j2\pi\theta}} = \frac{\sin(\mu\phi)e^{-j(\mu-1)\phi}}{\sin\phi},\tag{44}$$

where $\phi = \pi\vartheta = \frac{\pi}{N}(p - q + \nu_i + 2Nc_1\ell_i)$ is defined. Then, the modulus of $H_i[p, q]$ can be simplified as

$$\begin{aligned}|H_i[p, q]| &= \left| \frac{1}{\mu} e^{j\frac{2\pi}{N}(Nc_1\ell_i^2 - q\ell_i)} \mathcal{F}_i(p, q) \right| \\ &= \left| \frac{1}{\mu} e^{j\frac{2\pi}{N}(Nc_1\ell_i^2 - q\ell_i)} e^{-j(\mu-1)\phi} \frac{\sin(\mu\phi)}{\sin\phi} \right| \\ &= \left| \frac{\sin(\mu\phi)}{\mu \sin\phi} \right|.\end{aligned}\tag{45}$$

Expressing $\mu\phi = (\mu - 1)\phi + \phi$, $|H_i[p, q]|$ can be set to satisfy

$$\begin{aligned} |H_i[p, q]| &= \left| \frac{\sin((\mu - 1)\phi + \phi)}{\mu \sin \phi} \right| \\ &= \left| \frac{\sin((\mu - 1)\phi) \cos \phi}{\mu \sin \phi} + \frac{\cos((\mu - 1)\phi))}{\mu} \right| \\ &\leq \left| \frac{\sin((\mu - 1)\phi) \cos \phi}{\mu \sin \phi} \right| + \left| \frac{\cos((\mu - 1)\phi))}{\mu} \right|. \end{aligned} \quad (46)$$

Then, using the inequality $|\sin k\theta| \leq |k \sin \theta|$ for $k \geq 0$ and $\cos((\mu - 1)\phi) \leq 1$, we obtain

$$\begin{aligned} |H_i[p, q]| &\leq \left| \frac{(\mu - 1) \sin \phi \cos \phi}{\mu \sin \phi} \right| + \left| \frac{1}{\mu} \right| \\ &\leq \frac{\mu - 1}{\mu} |\cos \phi| + \frac{1}{\mu} \leq 1. \end{aligned} \quad (47)$$

The right hand side of (47) reaches its peak value 1, when $\phi = v\pi$ for integer v . From $\phi = \pi\theta = \frac{\pi}{N}(p - q + \nu_i + 2Nc_1\ell_i)$, we know that the peak occurs at $q = [(p + \eta_i)/N]$, where $\eta_i = [(\nu_i + 2Nc_1\ell_i)/N]$ is defined. As q moves away from this value, the right hand side of (47) decreases. Moreover, the larger the value of μ is, the faster is the decreasing of $|H_i[p, q]|$ with respect to q . Therefore, following the analysis in [3], we approximate $|H_i[p, q]|$ to be non-zero only for $2\zeta + 1$ values of q , which are centered at $q = [(p + \eta_i)/N]$. Specifically, ζ can be set to a value so that, for all i and p satisfying $|q - [(p + \eta_i)/N]| > \zeta$, the right hand side of (47) is smaller than a pre-set small threshold. Accordingly, the elements in \mathbf{H}_i have the values of

$$H_i[p, q] = \begin{cases} \frac{1}{\mu} e^{j\frac{2\pi}{N}(Nc_1\ell_i^2 - q\ell_i)} \mathcal{F}_i(p, q), & \text{if } [(p + \eta_i - \zeta)/N] \leq q \leq [(p + \eta_i + \zeta)/N], \\ 0, & \text{otherwise.} \end{cases} \quad (48)$$

Consequently, in the case of fractional Doppler shifts, the input-output relationship of the A²FDM can be represented as

$$\begin{aligned} r[p] &= \frac{1}{\mu} \sum_{i=1}^L \sum_{q=[(p+\eta_i-\zeta)/N]}^{[(p+\eta_i+\zeta)/N]} h_i e^{j\frac{2\pi}{N}(Nc_1\ell_i^2 - q\ell_i)} \\ &\quad \times \frac{1 - e^{-j\frac{2\pi}{N\mu}(p-q+\nu_i+2Nc_1\ell_i)}}{1 - e^{-j\frac{2\pi}{N}(p-q+\nu_i+2Nc_1\ell_i)}} s[q] + \tilde{w}[p] \end{aligned} \quad (49)$$

for $p = 0, 1, \dots, N - 1$.

IV. ANALYSIS OF THE EFFECT OF PARAMETERS AND COMPLEXITY

In this section, we first analyze the effect of parameters c_1 and μ on diversity gain, followed by the analysis of parameter μ on the PAPR.

A. Effect of Parameter c_1 on Diversity Order

For an AFDM having N subcarriers and maximum Doppler shift ν_{\max} to achieve full diversity gain, it was suggested [3] that the parameter c_1 is set to $c_1 = \frac{2\nu_{\max}+1}{2N}$. This choice of c_1 is based on the observation that, to achieve full diversity gain, any distinct multipath components should make contributions via occupying non-overlapping positions in the effective channel matrices. Specifically, when two multipath components, i and j , are considered, as shown in [3], the non-zero elements in \mathbf{H}_i and \mathbf{H}_j appear at the positions $[p, p + \eta_i]$ and $[p, p + \eta_j]$, respectively, where p is the row index and $\eta_k \triangleq [(\nu_k + 2Nc_1\ell_k)/N]$, $k = i$ or j , with $[(\cdot)/N]$ denoting the modulo- N operation. Then, to ensure the above-mentioned non-overlapping contributions made by components i and j in the effective channel matrix, the ranges covering η_i and η_j must be disjoint, i.e., satisfying

$$\begin{aligned} \{-\nu_{\max} + 2Nc_1\ell_i, \dots, \nu_{\max} + 2Nc_1\ell_i\} \cap \\ \{-\nu_{\max} + 2Nc_1\ell_j, \dots, \nu_{\max} + 2Nc_1\ell_j\} = \emptyset, \end{aligned} \quad (50)$$

where ν_{\max} is the maximum Doppler shift. Explicitly, this can be achieved, if c_1 is chosen to satisfy (17). If there are adjacent paths, meaning that $\min(|\ell_j - \ell_i|) = 1$, c_1 is chosen to meet

$$c_1 > \frac{2\nu_{\max}}{2N} \quad (51)$$

which is typically selected as $c_1 = (2\nu_{\max} + 1)/2N$.

The selection of c_1 based on (51) needs some channel knowledge of, at least ν_{\max} , which may be time-varying in practice. For example, when an unmanned aerial vehicle (UAV) accelerates or turns around, the maximum Doppler shift might be different. Based on (51), we may argue that the condition can be satisfied, provided that a large value of c_1 is chosen to cover all the possible Doppler ranges. However, (51) has been derived when the modulo- N operation in η_k is ignored. If the modulo- N operation is invoked, we will see that even when the condition of (51) is satisfied, two distinct multipath components may result in their contributions falling in the same location in the effective channel matrix, as shown below.

Since $\nu_i = f_i N = f_{Di} N / B$, where f_{Di} is the actual Doppler shift that is usually significantly smaller than B of system's bandwidth (or sampling rate), we can assume that $2\nu_{\max} < N$. Now, let us consider a c_1 that satisfies the condition of (51), but

$$\begin{aligned} \eta_i &= \nu_i + 2Nc_1\ell_i = \eta, \\ \eta_j &= \nu_j + 2Nc_1\ell_j = dN + \eta, \end{aligned} \quad (52)$$

where $0 \leq \eta \leq N-1$ and d can be any non-zero integer. Then, although the indices of η_i and η_j are separated by a distance of dN , due to the modulo- N operation, the contributions made by components i and j overlap in the effective channel matrix, hence, losing the diversity gain provided by multipath components i and j . Furthermore, upon substituting η from the first equation in (52) into the second one, we can realize that, provided that there exist multipath components i and j , whose associated quantities satisfy

$$c_1 = \frac{dN + \nu_i - \nu_j}{2N(\ell_j - \ell_i)}, \quad (53)$$

one of the diversity orders then becomes lost. Therefore and in summary, the condition of (51) for c_1 selection is necessary but not sufficient. Certain values of c_1 satisfying (51) may induce the overlaps of different multipath components in the effective channel matrix, resulting in the reduction of diversity gain, as demonstrated by the numerical results in Section V.

Note that, according to the 3GPP's specifications [38–40], in most practical applications, Doppler shifts usually do not exceed 10% of the subcarrier spacing, i.e., $\nu_i < 0.1$. This means that the term of $\nu_i - \nu_j$ in (53) is negligible compared to dN , making (53) approximately $c_1 \approx d/2(\ell_j - \ell_i)$. When c_1 takes this value, it can be found that the non-zero elements in the effective channel matrix contributed by the i th and j th components are located at $[p, p + \nu_i]$ and $[p, p + \nu_j]$, respectively, which are effectively indistinguishable due to the small difference between ν_i and ν_j . Moreover, if $c_1 \approx d/2 \min(|\ell_j - \ell_i|)$, such as, $c_1 \approx d/2$ is used, all the multipath components will approximately satisfy the conditions in (52). In this case, although c_1 is chosen to satisfy (51), the achieved diversity order will be reduced to approximately 1, regardless of L , the actual number of multipaths.

In contrast, our proposed A²FDM leverages both the chirp processing and precoding to achieve diversity gain. Specifically, each transmitted symbol is firstly spread onto N_μ subcarriers via the Γ_μ operator. Hence, in A²FDM systems with interleaved permutation, the achieved diversity order is $\min\{N_\mu, L\}$. Even when a c_1 is mistakenly chosen, leading to multipath component overlapping, the spreading by Γ_μ operator is still capable of preserving the full achievable diversity gain, as long as $N_\mu \geq L$. Otherwise, if $1 < N_\mu < L$, the achieved diversity order is still at least equal to N_μ , instead of being reduced to 1 in the conventional AFDM systems. Note that, if $N_\mu = 1$, A²FDM is reduced to the AFDM with $c_2 = 1$ or other integer.

In summary, while the diversity order achieved by AFDM may degrade to 1 under the unfavourable setting of c_1 , A²FDM can consistently guarantee a diversity order of $\min\{N_\mu, L\}$, reducing the cost paid for a wrongly selected parameter c_1 . When $N_\mu \geq L$, the value of c_1 has no impact on the performance of A²FDM, a full diversity gain can be guaranteed. If $N_\mu < L$, the full diversity gain can also be achieved, when c_1 is selected to meet the condition of (51) but not satisfy the condition in (53). Otherwise, if a wrong parameter c_1 is applied, the achieved diversity order is still guaranteed in the range of N_μ and L .

B. Effect of Parameter μ on PAPR

AFDM inherits the same PAPR problem of OFDM, with the PAPR being as high as N in an AFDM system with N subcarriers. Our A²FDM scheme enables substantial mitigation of the PAPR problem conflicted by AFDM.

Specifically, for the IA²FDM scheme addressed in Section III-A1, as shown in (30), there are only μ out of the N subcarriers activated at any time, with the μ subcarriers uniformly distributed within the N subcarriers. Similarly, for the LA²FDM considered in Section III-A2, as illustrated by (36), there are either μ or $(\mu+2)$ out of the N subcarriers activated, depending on the time instants within a symbol duration. Hence, in both IA²FDM and LA²FDM, the parameter μ can be adjusted to strike a trade-off between PAPR and implementation

complexity, as analyzed in the following section. For instance, if $\mu = 1$, IA²FDM activates only one subcarrier while LA²FDM activates three, regardless of the value of N . However, in this case, A²FDM needs to add most computation on AFDM. By contrast, when μ increases, signal's PAPR in A²FDM increases, but the extra computation invested above AFDM reduces. Nevertheless, as the extra computation is mainly from the blocks of FFT operations, the complexity of A²FDM added on AFDM is mild, as to be detailed in Section IV-C.

C. Complexity Comparison between A²FDM and AFDM

At transmitter, by comparing the \mathbf{A} matrices in AFDM and in A²FDM, which are $\mathbf{A} = \mathbf{\Lambda}_{c_2} \mathbf{F} \mathbf{\Lambda}_{c_1}$ for AFDM and $\mathbf{A} = \mathbf{\Upsilon}_\mu^H \mathbf{P}^T \mathbf{F} \mathbf{\Lambda}_{c_1}$ for A²FDM, we can readily know the extra computation required by A²FDM in comparison with AFDM. As shown in these formulas, to implement A²FDM, the matrix $\mathbf{\Lambda}_{c_2}$ is replaced by $\mathbf{\Upsilon}_\mu^H \mathbf{P}^T$. For AFDM transmitter, the complexity due to $\mathbf{\Lambda}_{c_1}$ and $\mathbf{\Lambda}_{c_2}$ can be ignored, making the complexity of AFDM is similar to that of OFDM, which is $\mathcal{O}(N \ln N)$, contributed by the N -point IFFT. For A²FDM transmitter, the complexity contributed by $\mathbf{\Lambda}_{c_1}$ and \mathbf{P} of permutation operation can also be ignored. Then, the complexity of A²FDM transmitter is given by that for computing the μ number of N_μ -point FFT and that for computing one N -point IFFT, yielding a complexity of $\mathcal{O}(N[\ln N + \ln(N/\mu)])$. Hence, the extra complexity of A²FDM transmitter above AFDM transmitter is $\mathcal{O}(N \ln(N/\mu))$, which reduces as μ increases¹. However, as discussed in Section IV-B, the PAPR of A²FDM signals increases, as μ increases, making a trade-off between the complexity of transmitter implementation and the PAPR of transmit signals.

At receiver, both AFDM and A²FDM require the equalization built on the signals received from N subcarriers. Accordingly, the inverse of a $(N \times N)$ matrix is required, for instance, if a MMSE-based equalizer is implemented. This equalizer dominates receiver's computation, having the complexity much higher than the N -point FFT. Hence, the computational loads for both AFDM and A²FDM receivers are similar.

V. PERFORMANCE RESULTS AND ANALYSIS

In this section, we present the simulation results to demonstrate the performance of our proposed A²FDM and compare it with the performance of AFDM. The main parameters used in simulations are the same as listed in Table I, unless otherwise specified. The delays of multipath components normalized by the sampling duration are randomly distributed in the integer set $[1, \ell_{\max} = 30]$, where ℓ_{\max} denotes the maximum normalized delay-spread. The Doppler shifts normalized by subcarrier spacing Δf is distributed in $[-\nu_{\max}, \nu_{\max}]$, set according to $\nu_l = \nu_{\max} \cos(\varphi_i)$ with φ_i uniformly distributed in $[-\pi, \pi]$. In the cases of achieving maximum diversity order, the value of parameter c_1 is typically set as $c_1 = c_{1f}$, as seen in (17), for both AFDM and A²FDMA, unless otherwise specified. For receiving equalization, the MMSE-assisted detection is employed.

¹Note that, more accurately, A²FDM transmitter also has the complexity of $\mathcal{O}(N \ln N)$ as $\mathcal{O}(N[\ln N + \ln(N/\mu)]) = c\mathcal{O}(N \ln N)$ considering $\mu < N$, where c is a constant. Hence, in comparison with AFDM, A²FDM only has some extra computation that is proportional to $\mathcal{O}(N \ln(N/\mu))$

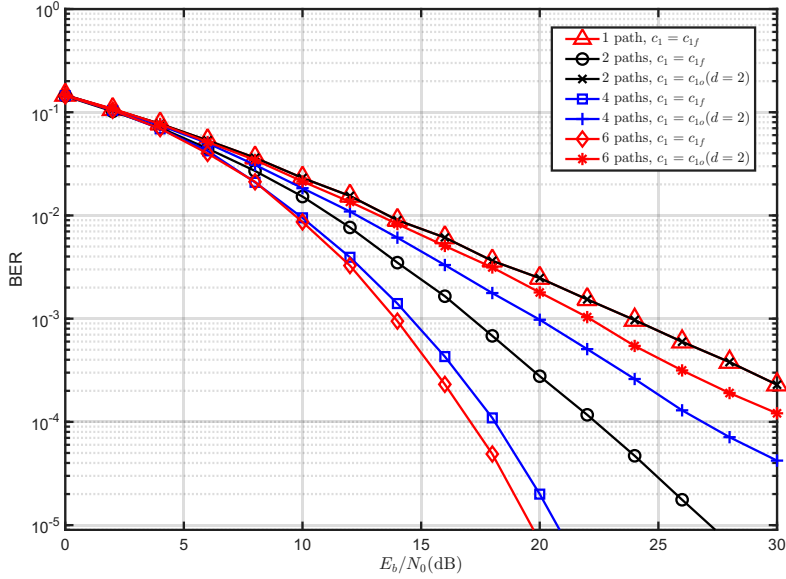


Fig. 7. Demonstration of the effect of c_1 on the BER performance of AFDM systems.

In Section IV-A, the analysis shows that an inappropriate value for c_1 may result in the loss of performance of the AFDM systems, although c_1 is set to satisfy (17) but also satisfies (53). This is shown in Fig. 2 in Section II-C and Fig. 7 here, when c_1 is set according to (53) with $d = 2$, labelled as $c_1 = c_{1o}(d = 2)$ in these figures. As shown in Fig. 2, most of the diversity gain is lost, although wireless channel has $L = 10$ paths. As shown in Fig. 7, the BER performance becomes unpredictable, with $L = 2$ yielding nearly the same performance as $L = 1$, and the BER performance of $L = 4$ is better than that of $L = 6$. In all these cases, the BER performance is much worse than that of the corresponding cases with $c_1 = c_{1f}$.

Correspondingly, in Figs. 8 and 9, the BER performance of the IA²FDM systems with relatively large $\mu = 128$ and small $\mu = 2$ is demonstrated. As seen in Fig. 8, for a given L of the number of paths, the BER performance is the same in the cases of employing both appropriate and inappropriate c_1 values. This is because the achieved diversity gain in the case of relatively large $\mu = 128$ is mainly determined by μ . By contrast, when $\mu = 2$, which is small, as shown in Fig. 9, the BER performance becomes similar as that shown in Fig. 7. However, when comparing the results shown in Fig. 9 and that in Fig. 7, if the value of c_1 is correctly set, both AFDM and IA²FDM attain the same BER performance. In contrast, when c_1 is wrongly set, the BER performance of IA²FDM is noticeably better than that of AFDM for both $L = 4$ and $L = 6$, in addition to the reduced PAPR in IA²FDM systems.

Fig. 10 illustrates the BER performance of the IA²FDM systems with configurations of $\mu = 1, 2, 4, 8, 16, 32, 64, 128$ and 256 , respectively. Accordingly, N_μ has the values of $N_\mu = 256, 128, 64, 32, 16, 8, 4, 2$, and 1 , respectively. As the baseline, the BER performance of the corresponding AFDM system is included. As shown in Fig. 10, the BER performance of IA²FDM systems is nearly the same as that of the AFDM scheme. When $\mu = 1$, from (18) in Section III-A, we can know that $\mathbf{A} = \Lambda_{c_1}$, and hence, IA²FDM is reduced to a single-carrier

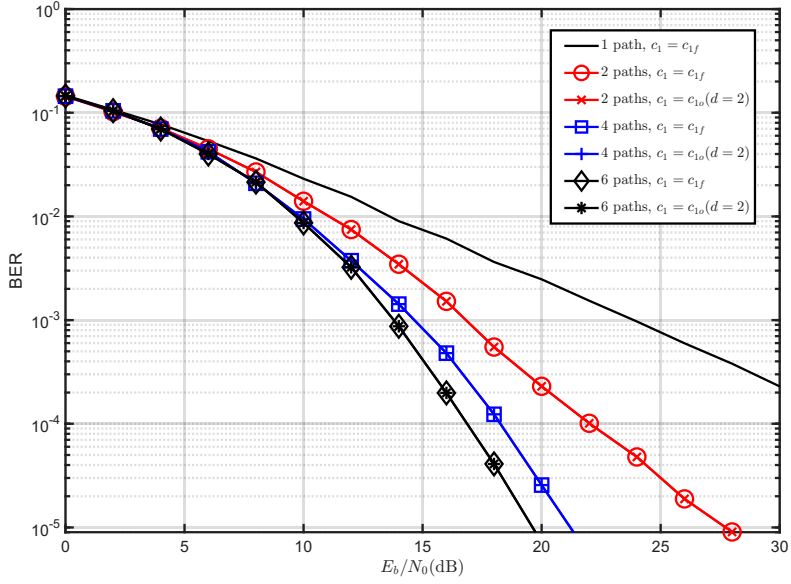


Fig. 8. Demonstration of the effect of c_1 on the BER performance of IA²FDM systems with μ set to a relatively large value of $\mu = 128$.

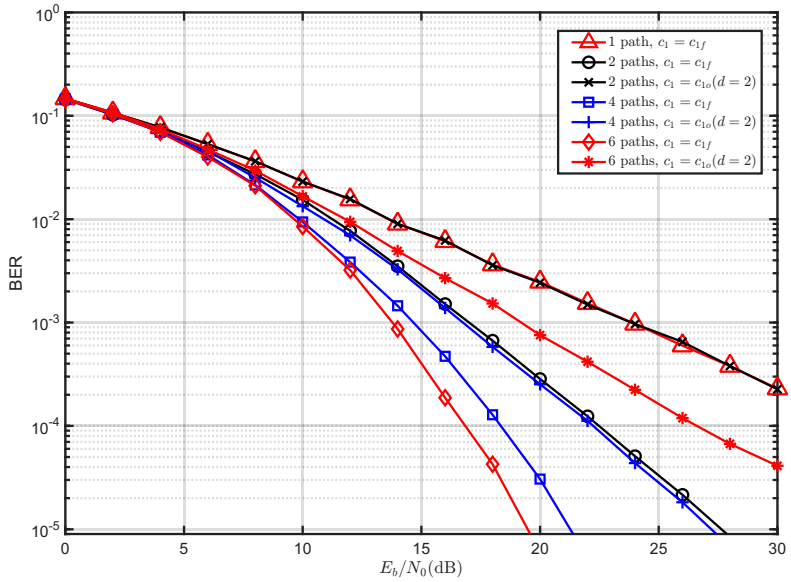


Fig. 9. Demonstration of the effect of c_1 on the BER performance of IA²FDM systems with μ set to a relatively small value of $\mu = 2$.

signalling scheme. This single-carrier system is expected to experience severer ISI. However, unlike the conventional single-carrier systems, the employment of CPP in IA²FDM effectively mitigates the ISI caused by the single-carrier signalling, enabling the system to achieve the comparable performance under both single-carrier and multi-carrier configurations.

Fig. 11 shows the BER performances of the LA²FDM systems with $\mu = 1, 2, 4, 16, 32, 64, 128$ and 256 , respectively, yielding corresponding $N_\mu = 256, 128, 64, 32, 16, 8, 4, 2$,

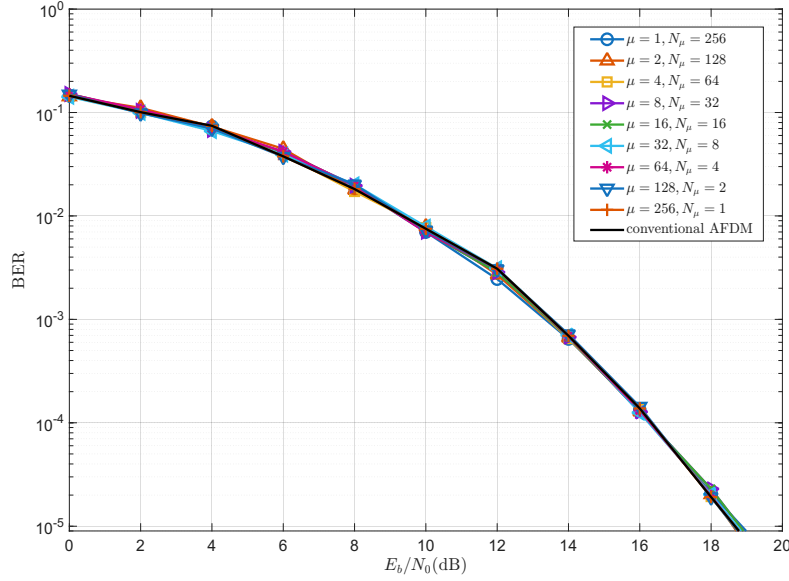


Fig. 10. BER performance of IA²FDM with $\mu = 1, 2, 4, 8, 16, 32, 64, 128$ and 256 , when $c_1 = c_{1f}$ is set.

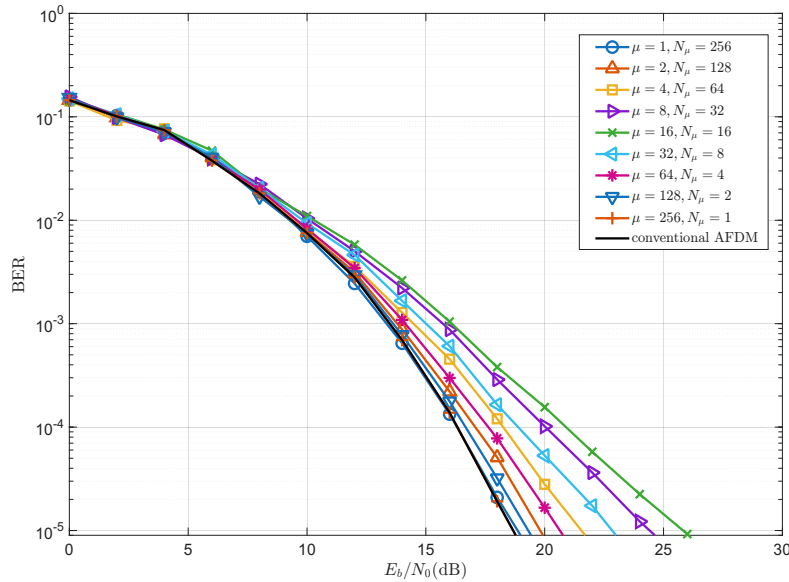


Fig. 11. BER performance of LA²FDM with $\mu = 1, 2, 4, 8, 16, 32, 64, 128$ and 256 , when $c_1 = c_{1f}$ is used.

and 1. Again, the BER performance of the AFDM attaining full diversity gain is provided as the benchmark. As shown by the results, the BER performance of LA²FDM first deteriorates as μ increases from $\mu = 1$ to $\mu = 16$, and then the BER performance improves as μ further increases, ultimately converging to that of the AFDM obtaining full diversity gain. The reason for the performance of LA²FDM systems as shown in Fig. 11 is as follows. First, with LA²FDM, a sub-block of data symbols, s_i , after FFT processing is assigned to adjacent subcarriers, which experience correlated fading. The diversity gain contributed by the operator Γ_μ in LA²FDM is usually only attainable when the number of subcarriers per

block, N_μ , is larger than L , a larger N_μ yields a higher diversity gain. Second, when μ is smaller, LA²FDM becomes more like single-carrier, yielding higher ISI, which degrades the BER performance of LA²FDM systems. Third, as μ increases or N_μ decreases, LA²FDM converges to AFDM, yielding reduced ISI with improved diversity gain due to the operation of Λ_{c_1} . After combining all the above-mentioned effects, the BER performance of LA²FDM systems first degrades, as μ increases, which is due to the reduced diversity gain contributed by the Γ_μ related operations, and then improves, as μ further increases, which is contributed by the diversity gain provided by the Λ_{c_1} relied operation.

Note that in LA²FDM, since the sub-blocks of data symbols are mapped to adjacent subcarriers experiencing correlated fading, the Γ_μ related operations, i.e., FFT and mapping, may not introduce diversity gain. However, this transmission scheme is beneficial to the downlink resource-allocation, where a sub-block of adjacent subcarriers, such as N_μ subcarriers, can be assigned to one downlink user. This downlink transmission scheme is usually capable of obtaining multiuser diversity gain, as different downlink users at different locations are expected to experience independent fading.

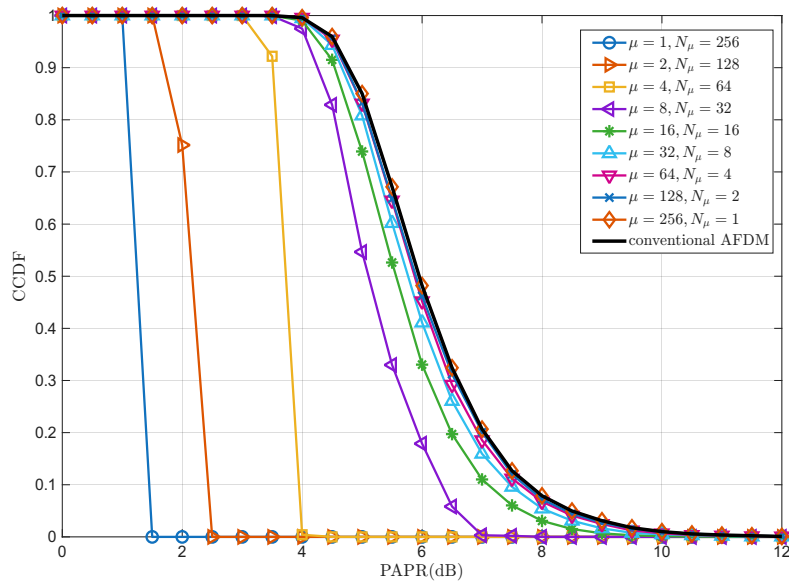


Fig. 12. CCDF of PAPR of the IA²FDM with $\mu = 1, 2, 4, 8, 16, 32, 64, 128$ and 256 .

Figs. 12 and 13 depict respectively the Complementary Cumulative Distribution Functions (CCDFs) of PAPR of the IA²FDM and LA²FDM for $\mu = 1, 2, 4, 8, 16, 32, 64, 128$ and 256 . For comparison, the CCDF of PAPR of the AFDM is included. When $\mu = 1$, both the IA²FDM and LA²FDM reduce to the single-carrier scheme, hence having the lowest PAPR. Otherwise, according to the analysis in Sections III-A1 and III-A2, the PAPR of both IA²FDM and LA²FDM increases with the increases μ , as explicitly seen in both figures, when μ is relatively small. By contrast, when the number of subcarriers is relatively big, which is 256 for the two figures, PAPR can be closely approximated by Gaussian distribution. Consequently, if μ is big enough, the PAPR's CCDFs of both the IA²FDM and LA²FDM converge to that

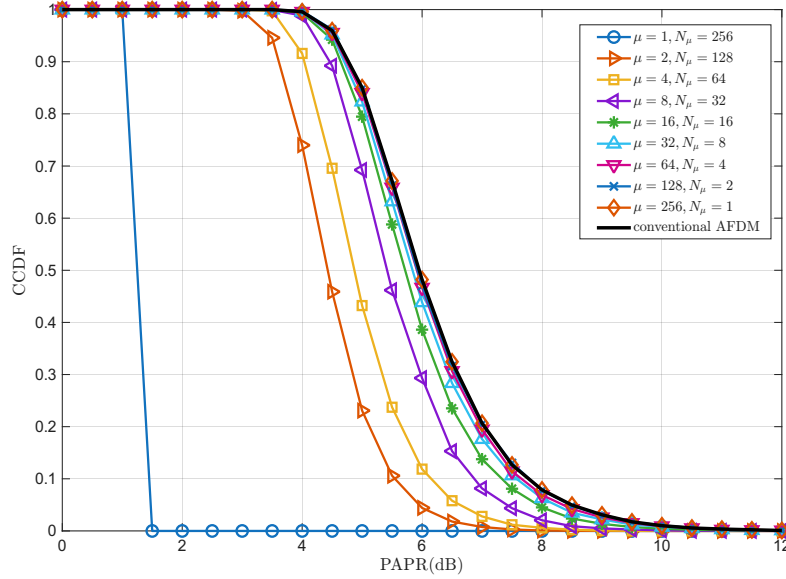


Fig. 13. CCDF of PAPR of the LA^2FDM with $\mu = 1, 2, 4, 8, 16, 32, 64, 128$ and 256 .

of the AFDM. However, we should note that although the distribution of PAPR of the AFDM becomes similar as that of the IA^2FDM and LA^2FDM , the worst PAPR of AFDM is still N , the number of subcarriers. In contrast, the worst PAPR of, for example, the IA^2FDM is only μ .

When comparing Fig. 12 and Fig. 13, we can see that, for a given μ - especially a given small value of μ , the PAPR of LA^2FDM is slightly higher than that of IA^2FDM , which agrees with our analysis in Sections III-A1 and III-A2.

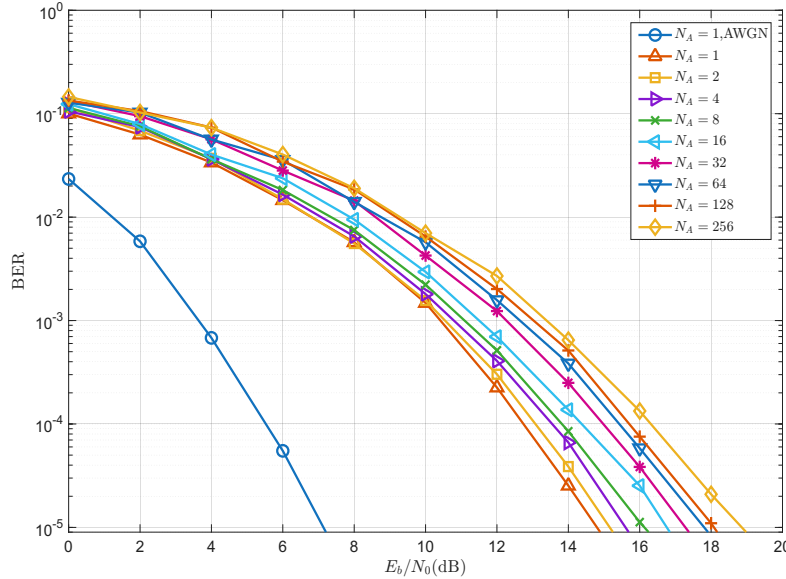


Fig. 14. Data rate and BER trade-off of the IA^2FDM systems with N_A out of N symbols activated for transmission, when $\mu = 1$ is assumed.

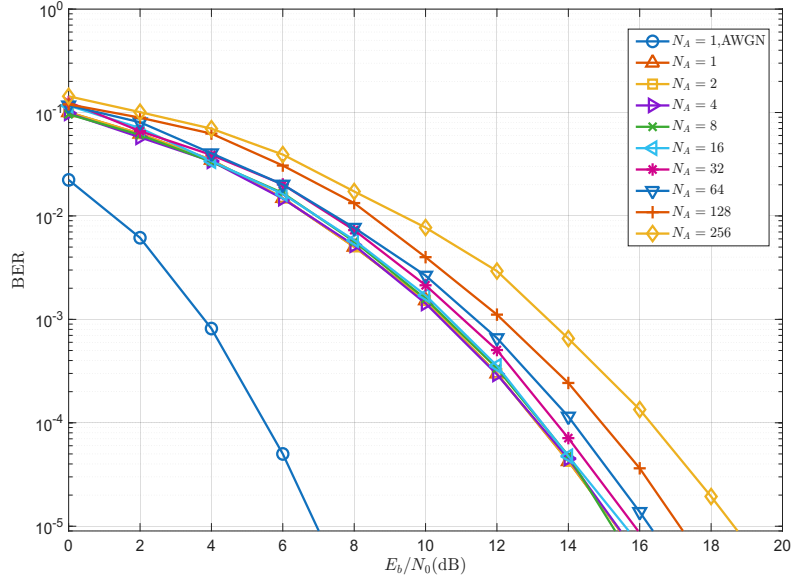


Fig. 15. Data rate and BER trade-off of the IA²FDM systems with N_A out of N symbols activated for transmission, when $\mu = 4$ is assumed.

Finally, in Figs. 14 and 15, the trade-off between data rate and diversity gain is demonstrated, when assuming $\mu = 1$ and $\mu = 4$, respectively, where the BER performance of 4QAM over Gaussian channel is also included for reference. Note that in these two figures, N_A From the principles of IA²FDM, and also of AFDM, we know that it experiences ISI, which needs to be sufficiently suppressed to obtain diversity gain. Higher ISI needs more resources, or more signal processing effort, to suppress, which may result in less diversity gain available for signal detection. In this example, activating more symbols generates higher ISI. Hence, when $N_A = 1$, there is no ISI. Hence, full diversity gain provided by the $L = 10$ -path double-selective fading channel can be obtained. Then, as N_A increases, which yields more ISI, the BER performance degrades, explicitly showing the trade-off between data rate and BER performance, or diversity gain.

When comparing Figs. 14 and 15, we can find that, except the cases of $N_A = 1, 2$, the IA²FDM with $\mu = 4$ provides better BER performance than the IA²FDM with $\mu = 1$ for all the other cases with $N_A > 2$. The reason behind is that the IA²FDM with $\mu = 1$ is a single-carrier scheme, while the IA²FDM with $\mu = 4$ uses 4 subcarriers to transmit at every time instant. Accordingly, in the IA²FDM with $\mu = 1$, all symbols are transmitted on one subcarrier at any time instant, while in the IA²FDM with $\mu = 4$, only one-fourth of symbols are transmitted on each of the four active subcarriers at any time instant. Consequently, when $N_A = 1$ or 2, meaning that there is no ISI or small ISI, the IA²FDM with $\mu = 1$ does not need to make much effort for ISI suppression and hence, can enjoy the near-full diversity gain. Otherwise, when $N_A > 2$, the IA²FDM with $\mu = 1$ is required to make more effort to suppress ISI than the IA²FDM with $\mu = 4$, which experiences less ISI owing to using 4 subcarriers at any time instant. Consequently, the IA²FDM with $\mu = 1$ attains reduced diversity gain, making its BER performance become worse than that of the IA²FDM with

$\mu = 4$.

VI. CONCLUSIONS

By replacing the diagonal matrix based on the unneeded parameter c_2 with a new unitary matrix that performs both sub-block-based DFT and symbol mapping, an A²FDM scheme was proposed to mitigate the PAPR problem conflicted by AFDM. Specifically, two symbol mapping schemes for A²FDM, yielding IA²FDM and LA²FDM, respectively, were proposed and investigated. Accordingly, the input-output relationships of IA²FDM and LA²FDM are derived, based on which the effect of parameter μ , denoting the number of DFT sub-blocks, is analyzed. The effect of parameter c_1 on the performance of AFDM and IA²FDM is analyzed to explain that the formula provided in literature for setting c_1 is only a necessary condition, but not sufficient. Furthermore, a comprehensive set of results were provided to demonstrate the impacts of involved parameters and to compare the performance of IA²FDM, LA²FDM and AFDM systems. Our analyses show that both IA²FDM and LA²FDM allow to circumvent the PAPR problem of AFDM. Owing to that the PAPR of both IA²FDM and LA²FDM is on the order of μ , instead of N of the total number of subcarriers. Hence, the PAPR of A²FDM signals can be configured according to practical application conditions, such as uplink, downlink, dynamic processing capability of transmitters, etc. Furthermore, while softening the PAPR problem of AFDM, the studies and results show that A²FDM also provides the design options, which are capable of guaranteeing the minimum diversity gain on the order of μ , and hence avoiding the loss of all the diversity gain in AFDM, in the cases when parameter c_1 happens to be a ‘bad’ value for some channel conditions.

Our future research issues on the topic will include investigating the other candidate symbol mapping schemes and their consequences, as well as studying A²FDM with integrated sensing and communications (ISAC).

APPENDIX A DERIVATION OF (35)

Upon substituting (23) into $x'_{(b\mu+a)}$, which is shown above (35), we obtain

$$\begin{aligned}
 x'_{(b\mu+a)} &= \frac{1}{\sqrt{N_\mu}} \sum_{p=0}^{N_\mu-1} z_{kN_\mu+p} e^{j2\pi \frac{p(b\mu+a)}{N}} \\
 &= \frac{1}{\sqrt{N_\mu}} \sum_{p=0}^{N_\mu-1} \frac{1}{\sqrt{N_\mu}} \sum_{l=0}^{N_\mu-1} s_{kN_\mu+l} e^{-j2\pi \frac{pl}{N_\mu}} e^{j2\pi \frac{p(b\mu+a)}{N}} \\
 &= \frac{1}{N_\mu} \sum_{l=0}^{N_\mu-1} s_{kN_\mu+l} \sum_{p=0}^{N_\mu-1} e^{j2\pi \frac{((b\mu+a)-l\mu)p}{N}}
 \end{aligned} \tag{54}$$

From (54) we have that, if $a = 0$, $n = b\mu$, and then $x'_n = x'_{(b\mu+a)}$ can be simplified to

$$\begin{aligned} x'_n = x'_{b\mu} &= \frac{1}{N_\mu} \sum_{l=0}^{N_\mu-1} s_{kN_\mu+l} \sum_{p=0}^{N_\mu-1} e^{j2\pi \frac{(b-l)\mu p}{N}} \\ &= \frac{1}{N_\mu} \sum_{l=0}^{N_\mu-1} s_{kN_\mu+l} \sum_{p=0}^{N_\mu-1} e^{j2\pi \frac{(b-l)p}{N_\mu}} \end{aligned} \quad (55)$$

Express $S_{bl} = \sum_{p=0}^{N_\mu-1} e^{j2\pi \frac{(b-l)p}{N_\mu}}$ and let $\psi = e^{j2\pi \frac{(b-l)}{N_\mu}}$. Explicitly, if $b = l$, then $\psi = 1$ and $S_{bl} = N_\mu$. By contrast, if $b \neq l$ and $\psi \neq 1$, we have $S_{bl} = \sum_{p=0}^{N_\mu-1} \psi^p = \frac{1-\psi^{N_\mu}}{1-\psi} = 0$. Expressing the above-mentioned in a compact form, if $a = 0$, we have

$$S_{bl} = \sum_{p=0}^{N_\mu-1} e^{j2\pi \frac{(b-l)p}{N_\mu}} = \begin{cases} N_\mu, & b = l \text{ (or } \psi = 1\text{)}, \\ 0, & b \neq l \text{ (or } \psi \neq 1\text{)}. \end{cases} \quad (56)$$

Accordingly, $x'_{b\mu}$ can be written as

$$\begin{aligned} x'_{b\mu} &= \frac{1}{N_\mu} \sum_{l=0}^{N_\mu-1} s_{kN_\mu+l} \times S_{bl} \\ &= \frac{1}{N_\mu} \left(s_{kN_\mu+b} \times N_\mu + \sum_{l=0, l \neq b}^{N_\mu-1} s_{kN_\mu+b} \times 0 \right) \\ &= s_{kN_\mu+b}. \end{aligned} \quad (57)$$

In the case of $a \neq 0$, x'_n can be simplified as

$$\begin{aligned} x'_n &= \frac{1}{N_\mu} \sum_{l=0}^{N_\mu-1} s_{kN_\mu+l} \left(\frac{1 - e^{j\frac{2\pi(n-l)\mu N_\mu}{N}}}{1 - e^{j\frac{2\pi(n-l)\mu}{N}}} \right) \\ &= \frac{1}{N_\mu} \sum_{l=0}^{N_\mu-1} s_{kN_\mu+l} \left(\frac{1 - e^{j2\pi(\frac{n}{\mu} - l)}}{1 - e^{j2\pi(\frac{n}{N} - \frac{l}{N_\mu})}} \right) \\ &= \frac{1}{N_\mu} \sum_{l=0}^{N_\mu-1} s_{kN_\mu+l} \left(\frac{1 - e^{j\frac{2\pi n}{\mu}}}{1 - e^{j\frac{2\pi n}{N}} e^{-j\frac{2\pi l}{N_\mu}}} \right). \end{aligned} \quad (58)$$

Consequently, when both $a = 0$ and $a \neq 0$ are considered, x'_n can be represented as (35).

REFERENCES

- [1] C. De Alwis, A. Kalla, Q.-V. Pham, P. Kumar, K. Dev, W.-J. Hwang, and M. Liyanage, "Survey on 6G frontiers: Trends, applications, requirements, technologies and future research," *IEEE Open Journal of the Communications Society*, vol. 2, pp. 836–886, 2021.
- [2] H. Yang, K. Zheng, K. Zhang, J. Mei, and Y. Qian, "Ultra-reliable and low-latency communications for connected vehicles: Challenges and solutions," *IEEE Network*, vol. 34, no. 3, pp. 92–100, 2020.
- [3] A. Bemani, N. Ksairi, and M. Kountouris, "Affine frequency division multiplexing for next generation wireless communications," *IEEE Transactions on Wireless Communications*, vol. 22, no. 11, pp. 8214–8229, 2023.
- [4] B. Li, F. Tong, J.-h. Li, and S.-y. Zheng, "Cross-correlation quasi-gradient Doppler estimation for underwater acoustic OFDM mobile communications," *Applied Acoustics*, vol. 190, p. 108640, 2022.

- [5] R. Hadani, S. Rakib, M. Tsatsanis, A. Monk, A. J. Goldsmith, A. F. Molisch, and R. Calderbank, “Orthogonal time frequency space modulation,” in *2017 IEEE Wireless Communications and Networking Conference (WCNC)*. IEEE, 2017, pp. 1–6.
- [6] L. Wu, S. Luo, D. Song, F. Yang, and R. Lin, “A message passing detection based affine frequency division multiplexing communication system,” *arXiv preprint arXiv:2307.16109*, 2023.
- [7] P. Raviteja, K. T. Phan, and Y. Hong, “Embedded pilot-aided channel estimation for OTFS in delay-Doppler channels,” *IEEE transactions on vehicular technology*, vol. 68, no. 5, pp. 4906–4917, 2019.
- [8] A. Bemani, N. Ksairi, and M. Kountouris, “AFDM: A full diversity next generation waveform for high mobility communications,” in *2021 IEEE International Conference on Communications Workshops (ICC Workshops)*. IEEE, 2021, pp. 1–6.
- [9] A. Bemani, G. Cuozzo, N. Ksairi, and M. Kountouris, “Affine frequency division multiplexing for next-generation wireless networks,” in *2021 17th International Symposium on Wireless Communication Systems (ISWCS)*. IEEE, 2021, pp. 1–6.
- [10] T. Erseghe, N. Laurenti, and V. Cellini, “A multicarrier architecture based upon the affine fourier transform,” *IEEE Transactions on Communications*, vol. 53, no. 5, pp. 853–862, 2005.
- [11] X. Ouyang and J. Zhao, “Orthogonal chirp division multiplexing,” *IEEE Transactions on Communications*, vol. 64, no. 9, pp. 3946–3957, 2016.
- [12] S.-C. Pei and J.-J. Ding, “Closed-form discrete fractional and affine Fourier transforms,” *IEEE transactions on signal processing*, vol. 48, no. 5, pp. 1338–1353, 2000.
- [13] Y. Zhou, H. Yin, J. Xiong, S. Song, J. Zhu, J. Du, H. Chen, and Y. Tang, “Overview and performance analysis of various waveforms in high mobility scenarios,” in *2024 7th International Conference on Communication Engineering and Technology (ICCET)*. IEEE, 2024, pp. 35–40.
- [14] V. Savaux, “DFT-based modulation and demodulation for affine frequency division multiplexing,” *Authorea Preprints*, 2023.
- [15] Y. Tang, A. Zhang, M. Wen, Y. Huang, F. Ji, and J. Wen, “Time and frequency offset estimation and intercarrier interference cancellation for AFDM systems,” in *2024 IEEE Wireless Communications and Networking Conference (WCNC)*. IEEE, 2024, pp. 1–6.
- [16] H. Yin and Y. Tang, “Pilot aided channel estimation for AFDM in doubly dispersive channels,” in *2022 IEEE/CIC International Conference on Communications in China (ICCC)*. IEEE, 2022, pp. 308–313.
- [17] W. Benzine, A. Bemani, N. Ksairi, and D. Slock, “Affine frequency division multiplexing for communications on sparse time-varying channels,” in *GLOBECOM 2023-2023 IEEE Global Communications Conference*. IEEE, 2023, pp. 4921–4926.
- [18] Y. Ni, Z. Wang, P. Yuan, and Q. Huang, “An AFDM-based integrated sensing and communications,” in *2022 International Symposium on Wireless Communication Systems (ISWCS)*. IEEE, 2022, pp. 1–6.
- [19] A. Bemani, N. Ksairi, and M. Kountouris, “Integrated sensing and communications with affine frequency division multiplexing,” *IEEE Wireless Communications Letters*, 2024.
- [20] Z. Sui, Z. Liu, L. Musavian, L.-L. Yang, and L. Hanzo, “Generalized spatial modulation aided affine frequency division multiplexing,” *IEEE Transactions on Wireless Communications*, pp. 1–1, 2025.
- [21] M. Qian, F. Ji, Y. Ge, M. Wen, and Y. L. Guan, “Generalized code index modulation aided AFDM for spread spectrum systems,” *IEEE Wireless Communications Letters*, pp. 1–1, 2025.
- [22] K. R. R. Ranasinghe, H. S. Rou, G. T. F. De Abreu, T. Takahashi, and K. Ito, “Joint channel, data and radar parameter estimation for AFDM systems in doubly-dispersive channels,” *IEEE Transactions on Wireless Communications*, 2024.
- [23] Y. Tao, M. Wen, Y. Ge, and J. Li, “Affine frequency division multiplexing with index modulation,” in *2024 IEEE Wireless Communications and Networking Conference (WCNC)*, 2024, pp. 1–6.
- [24] Y. Tao, M. Wen, Y. Ge, J. Li, E. Basar, and N. Al-Dhahir, “Affine frequency division multiplexing with index modulation: Full diversity condition, performance analysis, and low-complexity detection,” *IEEE Journal on Selected Areas in Communications*, vol. 43, no. 4, pp. 1041–1055, 2025.
- [25] G. Liu and et.al, “Pre-chirp-domain index modulation for full-diversity affine frequency division multiplexing toward 6G,” *IEEE Transactions on Wireless Communications*, vol. 24, no. 9, pp. 7331–7345, 2025.
- [26] Y. Rahmatallah and S. Mohan, “Peak-to-average power ratio reduction in OFDM systems: A survey and taxonomy,” *IEEE communications surveys & tutorials*, vol. 15, no. 4, pp. 1567–1592, 2013.
- [27] G. Surabhi, R. M. Augustine, and A. Chockalingam, “Peak-to-average power ratio of OTFS modulation,” *IEEE Communications Letters*, vol. 23, no. 6, pp. 999–1002, 2019.

- [28] P. Wei, Y. Xiao, W. Feng, N. Ge, and M. Xiao, “Charactering the peak-to-average power ratio of OTFS signals: A large system analysis,” *IEEE Transactions on Wireless Communications*, vol. 21, no. 6, pp. 3705–3720, 2021.
- [29] L.-L. Yang, J. Shi, K.-T. Feng, L.-H. Shen, S.-H. Wu, and T.-S. Lee, *Resource Optimization in Wireless Communications: Fundamentals, Algorithms, and Applications*. USA: Academic Press, 2025.
- [30] L.-L. Yang, *Multicarrier Communications*. John Wiley & Sons, 2009.
- [31] A. Bemani, N. Ksairi, and M. Kountouris, “Low complexity equalization for AFDM in doubly dispersive channels,” in *ICASSP 2022-2022 IEEE International Conference on Acoustics, Speech and Signal Processing (ICASSP)*. IEEE, 2022, pp. 5273–5277.
- [32] H. Yin and Y. Tang, “Pilot aided channel estimation for AFDM in doubly dispersive channels,” in *2022 IEEE/CIC International Conference on Communications in China (ICCC)*, 2022, pp. 308–313.
- [33] K. Zheng, M. Wen, T. Mao, L. Xiao, and Z. Wang, “Channel estimation for AFDM with superimposed pilots,” *IEEE Transactions on Vehicular Technology*, vol. 74, no. 2, pp. 3389–3394, 2025.
- [34] H. Ochiai and H. Imai, “Performance analysis of deliberately clipped OFDM signals,” *IEEE Transactions on communications*, vol. 50, no. 1, pp. 89–101, 2002.
- [35] R. W. Bauml, R. F. Fischer, and J. B. Huber, “Reducing the peak-to-average power ratio of multicarrier modulation by selected mapping,” *Electronics letters*, vol. 32, no. 22, pp. 2056–2057, 1996.
- [36] L. J. Cimini and N. R. Sollenberger, “Peak-to-average power ratio reduction of an OFDM signal using partial transmit sequences,” *IEEE Communications letters*, vol. 4, no. 3, pp. 86–88, 2000.
- [37] X. Li and L. J. Cimini, “Effects of clipping and filtering on the performance of OFDM,” in *1997 IEEE 47th Vehicular Technology Conference. Technology in Motion*, vol. 3. IEEE, 1997, pp. 1634–1638.
- [38] 3rd Generation Partnership Project (3GPP), “Study on channel model for frequencies from 0.5 to 100 GHz,” 3GPP, Technical Report TR 38.901, 2025, release 19.
- [39] 3rd Generation Partnership Project (3GPP), “NR physical channels and modulation,” 3GPP, Technical Specification TS 38.211, 2025, release 19.
- [40] 3rd Generation Partnership Project (3GPP), “Study on scenarios and requirements for next generation access technologies,” 3GPP, Technical Report TR 38.913, 2025, release 19.